AD-A129 945 THEORETICAL AND SEMI-EMPIRICAL METHODS OF DESIGNING 1/1
RIBBON UNWINDERS(U) THREE C SYSTEMS INC WYNNEWOOD PA
01 JUN 82 DAAK10-80-C-0297

UNCLASSIFIED F/G 19/1 NL

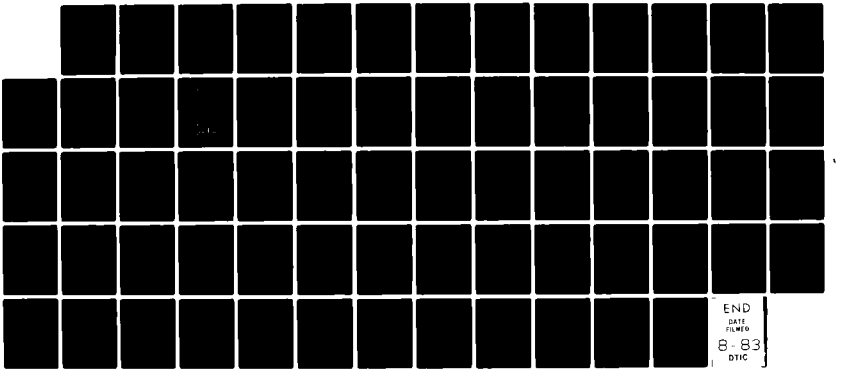

END
DATE FILMED
8-83
DTIC

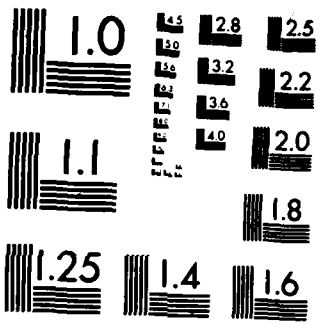

1 June 1982

# THEORETICAL AND SEMI-EMPIRICAL METHODS OF DESIGNING RIBBON UNWINDERS

FINAL REPORT: Contract DAAK10-80-C-0297

For: DEPARTMENT OF THE ARMY
U.S. ARMY ARMAMENT R&D COMMAND
SMALL CALIBER WEAPON SYSTEMS LABORATORY
DOVER, NEW JERSEY 07801

By: 3C Systems, Inc.
620 Argyle Road
Wynnewood, Pa. 19096

Hamilton Technology, Inc.
Lancaster, Pa.

Adaptronics, Inc.
McLean, Va.

TABLE OF CONTENTS


| | | Page |
|---|---|---|
| 1. | INTRODUCTION & SUMMARY | 1 |
| 2. | EXPERIMENTAL PROGRAM | |
| 2.1 | Test Plan | 9 |
| 2.2 | Ribbon Unwinder Assembly | 9 |
| 2.3 | Spinner Construction and Operation | 12 |
| 2.4 | Test Results and Data | 16 |
| 3. | MULTIVARIATE REGRESSION ANALYSIS BY ALN METHOD | |
| 3.1 | Discussion of the Data | 22 |
| 3.2 | Adaptive Learning Network Model | 26 |
| 3.3 | Discussion of Results | 31 |
| 4. | ANALYTICAL MODELS OF UNWINDER DYNAMICS | |
| 4.1 | The Straight Bridge Model | 33 |
| 4.2 | The Standing Wave Model | 44 |
| 4.3 | Correlations with Empirical Data | 48 |
| 4.4 | Predictive Formula for Unwinding Time | 52 |
| 5. | CONCLUSIONS & RECOMMENDATIONS | 55 |
| APPENDIX A - | ADAPTIVE LEARNING NETWORK METHOD | 58 |
| REFERENCES | | 64 |




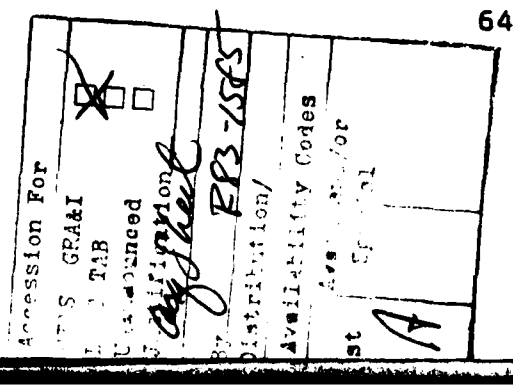

## 1. INTRODUCTION & SUMMARY

The objective of this program has been to develop theoretical and semi-empirical methods to enable engineers to design ribbon unwinders with reasonable accuracy and a minimum of development effort. This basic objective has been fulfilled, despite the fact that the degree of predictive accuracy depends to some extent on the design details of the fuze containing the ribbon unwinder. → Fig. 1 illustrates this point in relation to application of the unwinder principle to the XM579 Fuze.

Fig. 1 contains a cross-section (Section B-B) of the XM579 unwinder prior to spin-up. The ribbon is shown unrestrained, with a short length of its end free. There are surface adhesion forces developed during the ribbon winding process that are high enough to permit the coils to be handled in this manner, depending on ribbon material and surface finish and on winding tightness. When the projectile is fired, setback accelerations and friction provide the means whereby the ribbon coil is spun up to the projectile's rotation rate, and the tightness of a coil wound in the proper direction (opposite to the direction of spin) will increase during the spin-up period. After the spin-up period, centrifugal forces serve to unwind the coil and transfer it from the hub radially outward to the housing. When the detent pin is released by the innermost coil of the ribbon, it tumbles outward thereby releasing the rotor, which is turned to the armed position by centrifugal force.

Although winding tightness has been found not to be a significant parameter affecting arming time, and

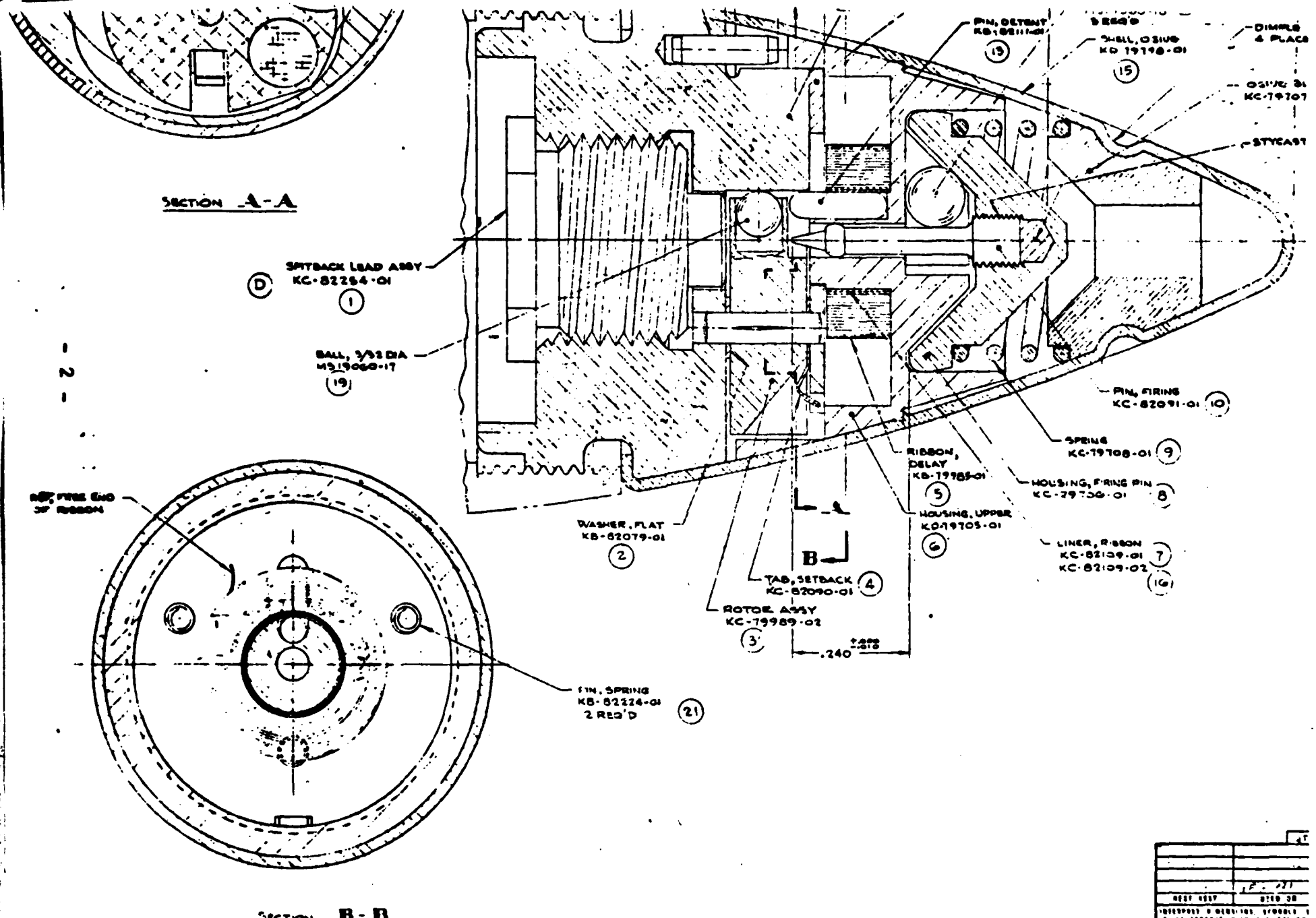


FIG. 1 XM579 FUZE

therefore the added tightening due to spin-up is expected not to be significant, the XM579 design feature of using a detent pin is expected to influence unwinding time. In the course of experimentation on this program, analysis of high speed films showed clearly that the radial pressure of the split-ring-hub used in the tests was the cause of some additional time delay, of the order of 10 milliseconds, after all but the innermost ribbon coil had been transferred out to the housing. It is therefore expected that the XM579 detent pin will provide a different time delay at the end of ribbon unwinding. For practical reasons like this, then, one cannot expect to develop completely general predictive equations for ribbon unwinding time, applicable to all fuze designs. Furthermore, if the ribbon is used to generate energy or to actuate other arming mechanisms, the external forces can be expected to result in additional time delays. Fortunately, however, practical delay systems can be designed without introducing excessive time delays above those provided by the pure unwinding process.

In order to fulfill the program objectives, a three-pronged investigation was undertaken, as follows:

(1) An experimental program employing wide variations in the parameters that affect ribbon unwinder performance. These parameters involved the ribbon geometric factors of thickness, width, length, hub radius and cavity radius; ribbon material parameters of density, modulus of elasticity, heat treatment, friction coefficient; loading factors of centrifugal loading and axial forces. It was originally planned to modify XM579 fuzes and fire them in 30mm rounds, in order to include any effects of axial loads during setback.* However, the modifications required to provide

* It was anticipated that very thin, very soft ribbons like lead might have their edges distorted during setback.

in-flight indications of the completion of arming were found to be far more expensive than this program could afford. Accordingly, the program objectives were accomplished in the laboratory using a high-speed air spinner. This change in experimental approach had its compensating virtue of permitting photographic observation of the ribbon dynamics as they unwound.

(2) A multivariate regression computer analysis of the experimental results in order to identify(on the basis of data alone, not theoretical nor intuitive expectations) critical parameters and combinations of parameters that could not be studied by analytical methods. Besides identification, this computational approach can quantify the dependency of ribbon unwinding time on these parameters for use in design.

(3) A theoretical analysis to obtain predictive equations involving the key parameters that affect unwinder performance. In a sense, this approach of analyzing the physics of unwinding and the above approach of computer analysis of experimental data alone could be considered competitive, perhaps yielding identical results. In practice, however, the approaches complement one another. The physical analysis can develop the general form of the unwinding time equation, including parameters that are not varied during the test series (in this instance, for example, hub radius and cavity radius were held constant), while the data-alone analysis cannot indicate the effects of parameters that are not varied. Multivariate regression analysis of the data does, on the other hand, include the effects of parameters that exist during testing but are not included in the physical analysis. Variations in test procedures and parameters that the physical analyst either could not

include in the analysis or did not expect to be important, may be uncovered by the multivariate regression analysis of the test data.

Selection of parameters for testing and analysis was made after study of the literature available on previous ribbon unwinder programs. Ref. 3 provided background on coiled steel ribbons that were attached to a high inertia pointer to indicate unwinding time. Because these ribbons functioned as springs and because of the high external inertia loading, these data could not be applied to the current unwinder program which uses unloaded, dead-soft ribbons.

Ref. 2 contains some useful data on brass ribbons fired at about 75,000 rpm in 20mm projectiles at heavy aluminum targets designed to stop the round's rotation on impact and to permit recovery of the unwinder ribbons. Fig. 2 contains these data. The approximately linear shapes of the curves in Fig. 2 are in agreement with those observed in this current program using high speed photography. One interpretation of the physical significance of a linear unwrapped length vs. time, or constant unwrapping velocity, curve is that the absence of accelerations indicates that inertia effects (ribbon density, for example) are not significant. The data of Fig. 2 are discussed further in Section 4.3 of this report.

The data provided in Ref. 1 are of great importance, having been obtained by high speed spinner tests using XM579 housings and with some of the identical aluminum ribbons (.004 inch or .102 mm thick, 22.5 inches or 572mm long) used in this program. The great majority of the tests were run with aluminum ribbons with thicknesses from .003

FIG. 2 FIRING TEST DATA FOR BRASS RIBBONS, T362 FUZE

Tevelow, F.L. "Terminal Report - T362 Octopus Fuze" DOFL Report TR-673 10 August 1959

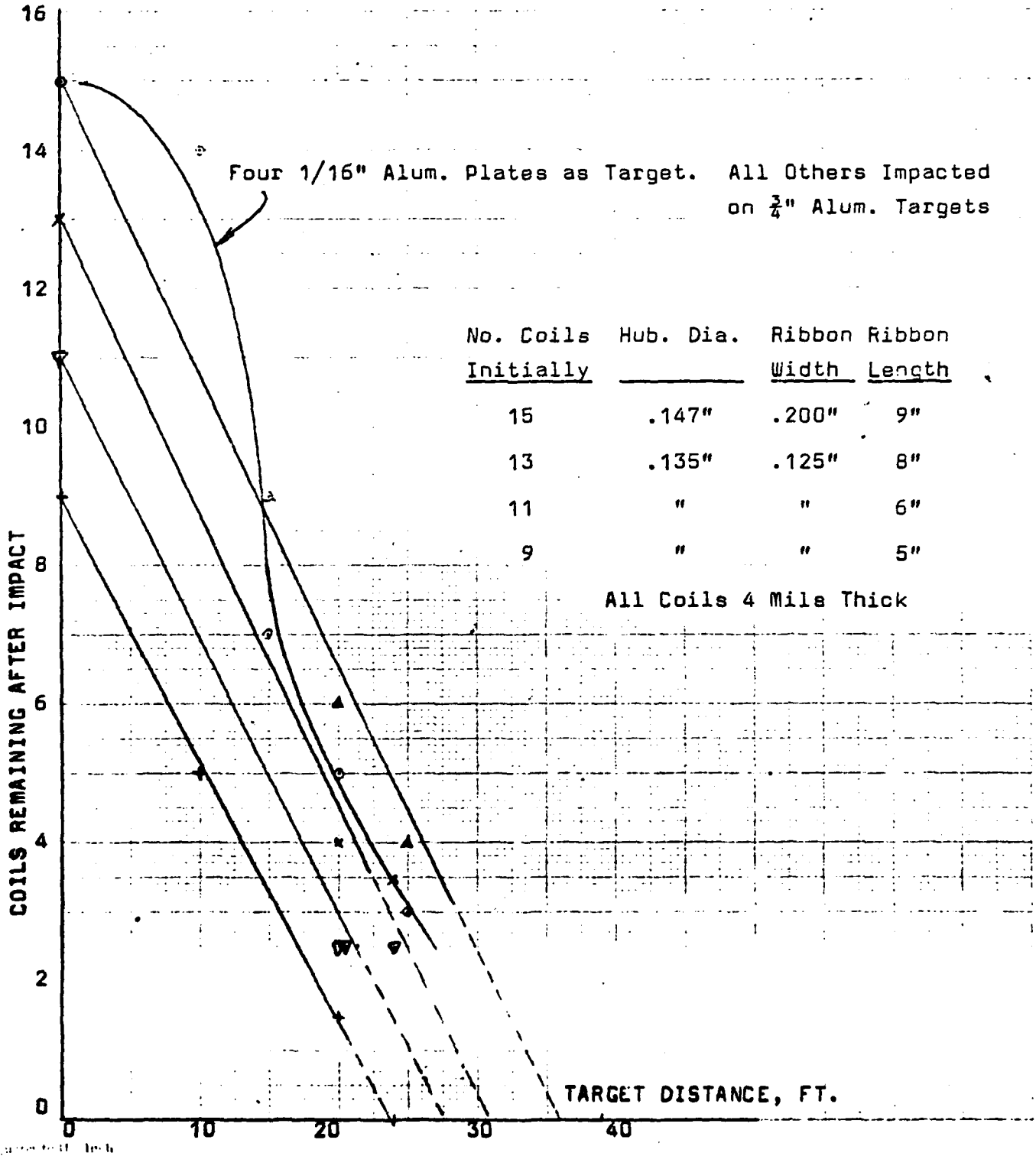


| No. Coils Initially | Hub. Dia. | Ribbon Width | Ribbon Length |
|---|---|---|---|
| 15 | .147" | .200" | 9" |
| 13 | .135" | .125" | 8" |
| 11 | " | " | 6" |
| 9 | " | " | 5" |

All Coils 4 Mils Thick

inches (.076mm) to .006 inches (.152mm), but some tests used gilding metal ribbons with much higher density. Despite great scatter in the data and inconsistencies between groups of data, the following trends could be noted:

(1) To a first approximation, neither ribbon density nor thickness nor spin rate affected unwinding time.

(2) Unwinding time was inversely proportional to ribbon length.

(3) The use of two .010 inch (.254mm) thick Teflon liners between the hub and the inner coil of the ribbon increased the unwinding time by an increment of the order of 13 milliseconds over the unwinding time of identical ribbons without liners.

This current program was designed to improve on the unsystematically obtained and often conflicting data gathered in previous programs. Ribbon dimensional and material parameters were varied over wide ranges, as were the external inputs of wrapping tightness and spin rate. Some of the preliminary conclusions reached previously were confirmed and others were refuted, as follows:

(1) Ribbon materials had to be in a dead soft condition to be suitable for unwinder application. Aluminum, brass, copper and lead were found to work well, but steel and titanium could not be annealed sufficiently to remain wound in a coil without external restraint. Lead was used successfully in the laboratory test program, but it is generally considered too soft a material to be handled in an operational fuze application.

(2) Ribbon material properties and thickness had no

definite effect on unwinding time.

(3) Winding tightness had no definite effect on unwinding time.

(4) Unwinding time was found to be proportional to ribbon length divided by spin rate-times-cavity radius, as given by Equation 28 in Section 4.4.

(5) For all the empirical data gathered in this air spinner test program, the standard deviation was 39 percent of the mean unwinding time. This is not considered excessive variation for an arming delay system.

Design equations for unwinding time and arming distance are given in Section 4.4 of this report. With the exception of corrections that may be introduced by the setback environment or by additional forces required to actuate specific arming mechanisms, these equations are considered adequate for the design of practical ribbon unwinder arming systems.

## 2. EXPERIMENTAL PROGRAM

### 2.1 Test Plan

Some of the parameters that were expected to have some influence on unwinding time of a ribbon are ribbon length and thickness and material (density, modulus of elasticity, inter-coil friction, etc.), winding tension spin rate, hub radius, and cavity radius. The latter parameters were held constant at .136 inches (3.45mm) .342 inches (8.69mm), respectively, since XM579 hardwa was adapted for use in the test spinner, and the other parameters were varied within the following limits:

Ribbon length: 10-30 inches (254-762mm)

Ribbon thickness: .0012-.004 inches (.0305-.102mm)

Materials: Aluminum, beryllium-copper, brass, copper, lead.

Winding tension: 20-570 grams

Spin rate: 20,000-33,000 rpm

An excessive number of tests would have been required to isolate the effects of variations in each parameter while all other parameters are held constant. Instead, a randomized-value test plan was designed, as described in Section 3. With this plan of approximately seventy tests (see Table 1), it is possible to determine the influence of each parameter, using a multivariate regression analysis of the data.

### 2.2 Ribbon Unwinder Assembly

A ribbon unwinder assembly consists of a two-piece

or split hub around which is wrapped a number of turns of a thin metal foil. See Fig. 3 below.

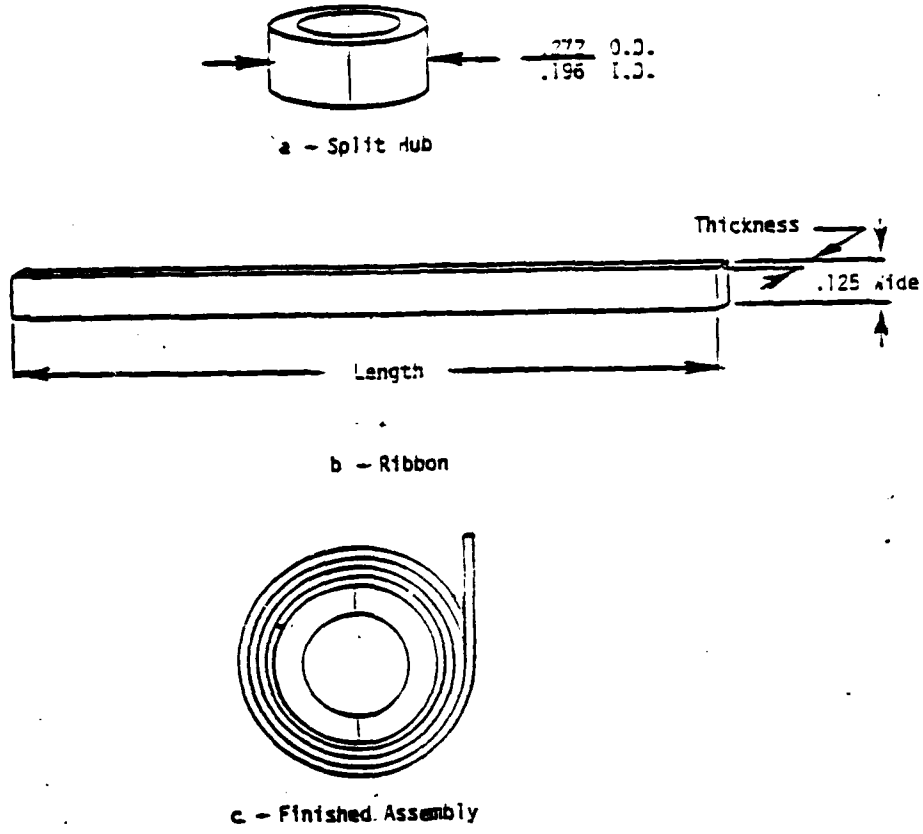


FIG. 3 RIBBON UNWINDER ASSEMBLY

The tape or ribbon of all unwinder assemblies was .125 inches (3.18mm) wide. The length and thickness of the tape was varied as shown in Table 1. Ribbon unwinder assemblies were fabricated in the laboratory using a simple hand crank mechanism to wind the ribbon onto the split hub. See Fig. 4.

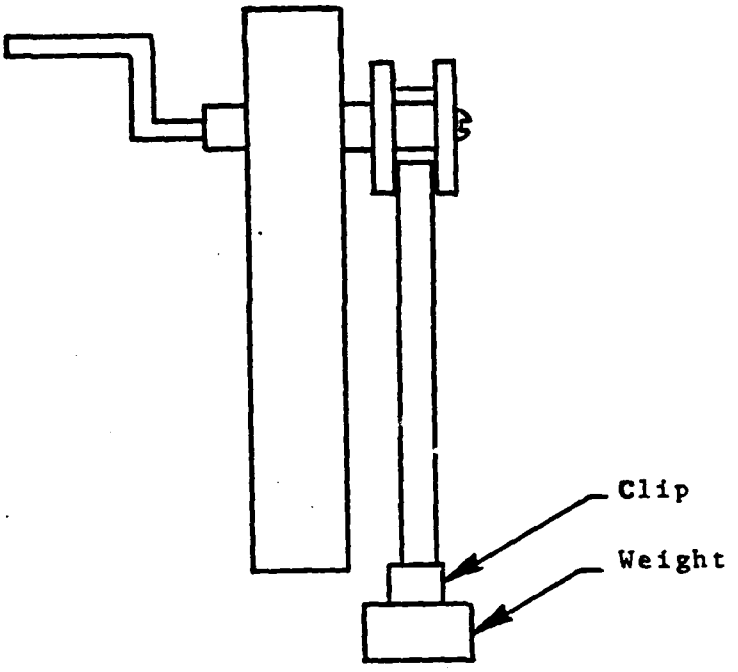


FIG. 4 HAND CRANK WINDING MECHANISM

Tension was maintained on the ribbon by means of a weight attached to its free end. It was necessary to apply a thin coat of magnesium oxide (milk of magnesia) to one side of all ribbons made from aluminum, beryllium copper, copper and brass. The magnesium oxide was applied by means of a cotton swab during the winding operation and was needed to prevent adjacent layers of the ribbon from sticking to one another during the annealing process. Ribbon assemblies made from the aforementioned materials were annealed in the wound condition by encasing each one individually in a special stainless steel form. Ribbon assemblies using lead or aluminum 1100-0 did not require annealing as they were soft enough to hold form in the as-wound condition.

Aluminum 1100-0 ribbons were obtained from fifty inert XM579 fuzes supplied to Hamilton Technology, Inc. (HTI) at the beginning of the program. HTI discovered that it was possible to rewind and retest a 1100-0 ribbon several times without degrading its timing characteristics. The aluminum ribbons were relatively easy to rewind, due to the dead soft condition of the aluminum.

Attempts were made to anneal steel and titanium ribbons, but they would not remain wound on the unwinder assembly. Accordingly, these materials were not employed in the test program.

## 2.3 Spinner Construction and Operation

Figure 5 shows a cutaway view of the laboratory spinner which was built at Hamilton Technology and which was used to obtain the experimental data. The high speed spinner is powered by a miniature air driven motor with speed controlled by regulated air pressure. An on-off air toggle switch is connected into the air inlet line to provide for additional air control. The air driven motor is coupled to the spinner on a one-to-one basis and the speed of the system is monitored by a Hewlett-Packard Model 5300A measuring system to which is fed signals from the light-photocell assembly at the aft end of the air motor.

Figure 5a shows the spinner without a ribbon unwinder assembly. Figure 5b shows the spinner with a ribbon unwinder assembly in place with the retainer screwed down on top of the split hub of the unwinder assembly. Figure 5c shows the spinner with the ribbon completely unwound and the two halves of the split hub thown clear of the main control shaft.

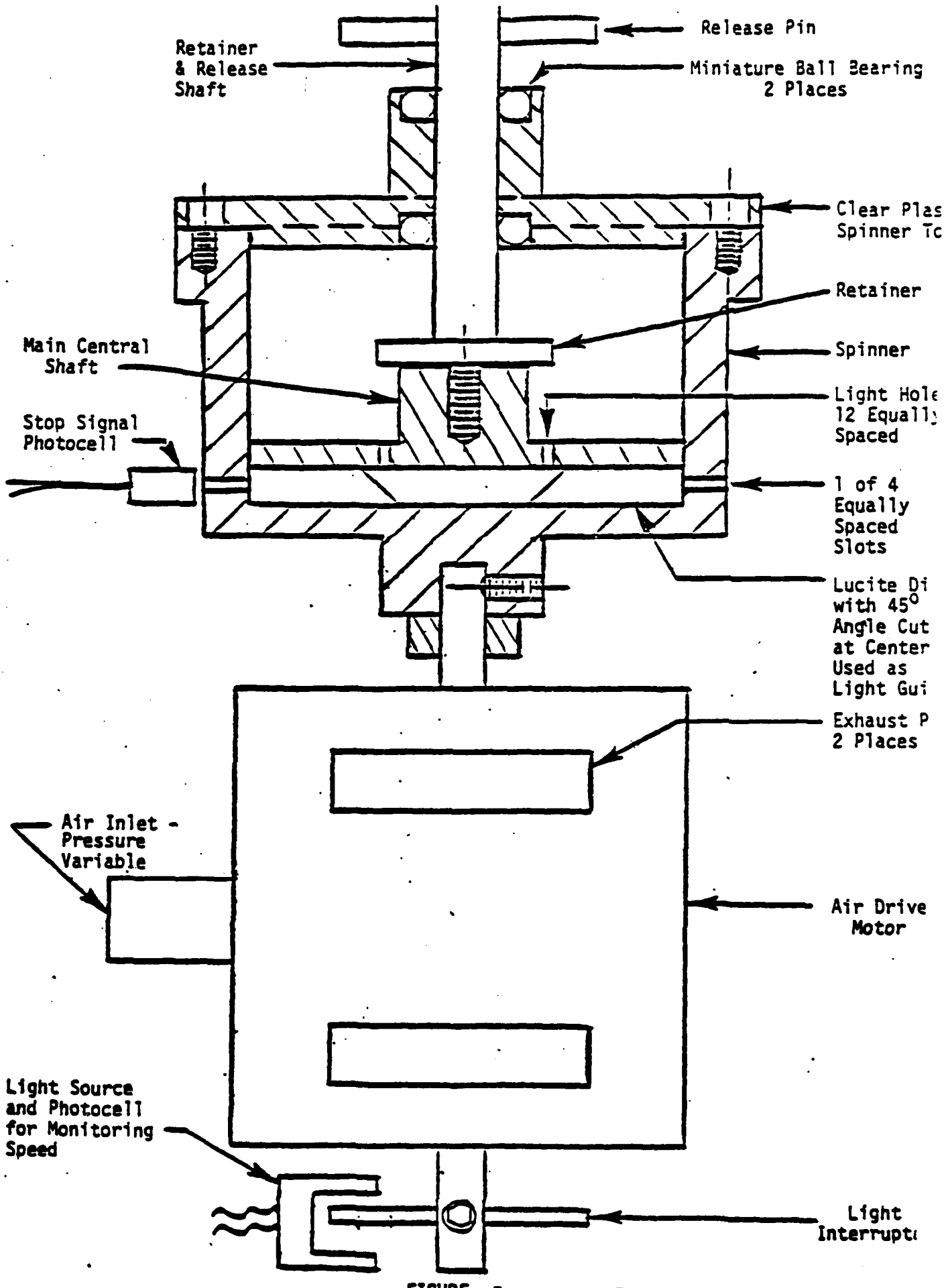
Release Pin
Retainer & Release Shaft
Miniature Ball Bearing 2 Places
Clear Plas Spinner Tc
Retainer
Main Central Shaft
Spinner
Light Hole 12 Equally Spaced
Stop Signal Photocell
1 of 4 Equally Spaced Slots
Lucite Di with 45° Angle Cut at Center Used as Light Gui
Exhaust P 2 Places
Air Inlet - Pressure Variable
Air Drive Motor
Light Source and Photocell for Monitoring Speed
Light Interrupt

FIGURE 5a

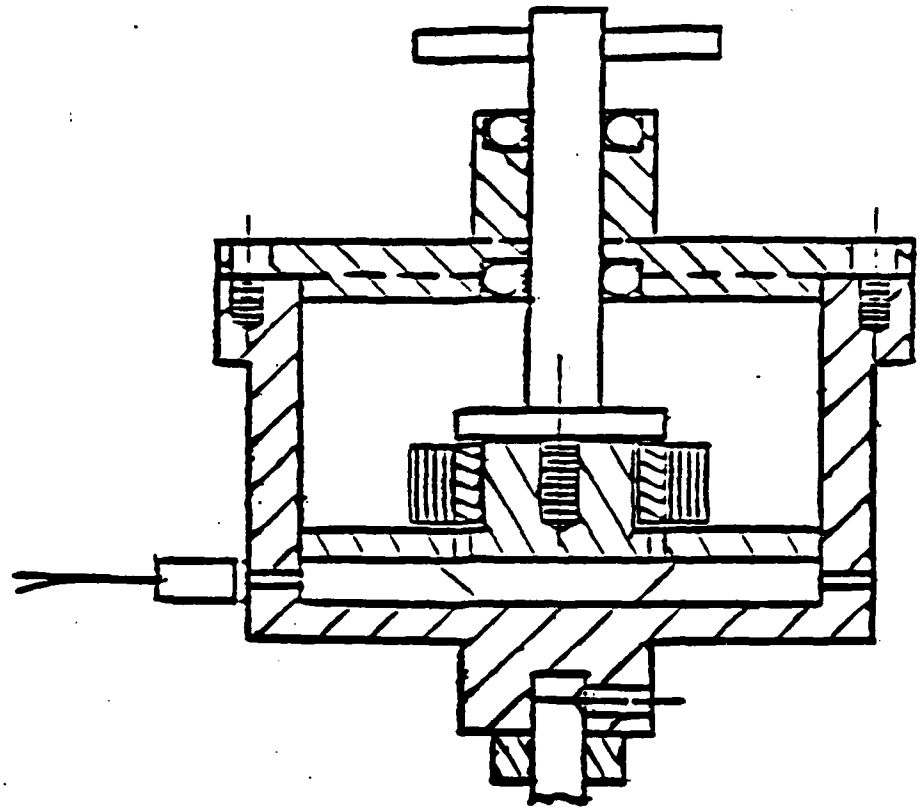

Figure 5b

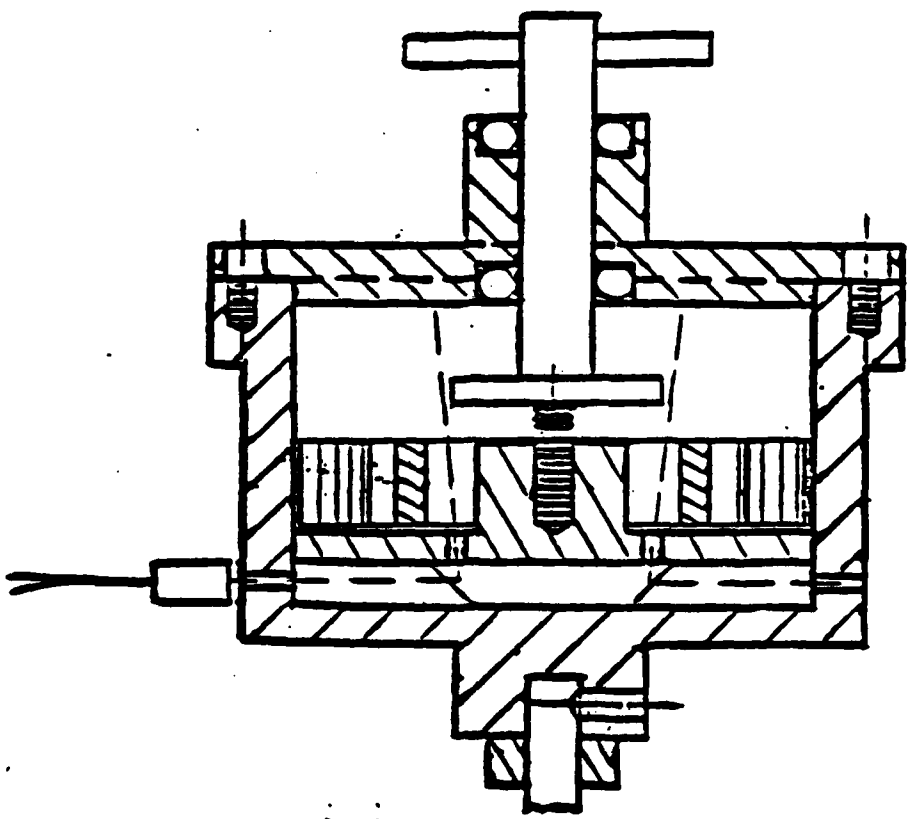

Figure 5c

With the ribbon unwinder in place in the spinner, as shown in Fig. 5b, the air motor is accelerated until the desired speed is obtained. At this time, a mechanical interrupter, not shown, contacts the tip of the release pin causing the retainer and release shaft to move counter-clockwise, which is opposite to the clockwise spin of the spinner. At the same time, the retainer backs off from the split hub and a start signal is sent to an electronic timer. Once the split hub has been freed of the pressure of the retainer, the entire ribbon unwinder assembly starts to rotate around the main central shaft of the spinner until all of the ribbon unwinds as shown in Fig. 5c.

In the absence of friction between the ribbon and the cavity wall onto which it is being transferred, it is possible for unwinding to occur even if the hub is not allowed to rotate. This form of unwinding can occur if the free end of the coil can slide freely inside the cavity wall, allowing the point of tangency with the hub to change. In actual operation, only a small amount of ribbon was transferred to the cavity wall before friction prevented further unwrapping. In four tests of aluminum ribbons at 25,900-33,900 rpm, the number of loops transferred to the cavity wall before hub release varied between $\frac{3}{4}$ and 2. Since these pre-release loops represent only a small fraction of the many loops to be transferred, this method of releasing the coil was considered accurate enough.

During the test, a concentrated beam of light is focused on the top of the spinner. This beam of light passes through the clear plastic spinner top and is blocked from further travel to the stop-signal photocell

by the split hub of the ribbon unwinder assembly. However, once the ribbon has completely unwound and the two halves of the split hub spin away from the main central shaft, the light proceeds along a path shown by the dotted line in Fig. 5c. When light hits the stop-signal photocell, a stop signal is transmitted to the electronic timer. The time between the start and stop signals to the electronic timer is the time delay of the ribbon unwinder.

## 2.4 Test Results and Data

Table 1 contains the test data obtained with the air spinner.

In addition to the unwinding times recorded in Table 1, several ribbons were observed with high speed photography as they unwound. Fig. 6 shows the results of a frame-by-frame analysis of the films. Resolution was not adequate to count the .004 inch (.102mm) thick coils; instead, the thickness of the ribbon bundle remaining on the split ring was measured. Several important observations may be made:

(1) The unwinding process is fairly linear, which implies that ribbon length is transferred at approximately a constant velocity during unwinding.

(2) There may be some time delay as the split ring pushes on the innermost ribbon coil, until its final release.

(3) The curve for Ribbon No. 2, wound in the wrong* direction(in the direction of rotation), shows a distinctly

---

* In Ref. 1, it is emphasized that ribbons wound in this way can be expected to produce unreliable results.

| NO. | MATERIAL | THICKNESS INCHES | LENGTH INCHES | TENSION GRAMS | SPINNER RPM | TIME MILLISEC'S. | REMARKS |
|---|---|---|---|---|---|---|---|
| 3/11/82 | | | | | | | |
| 1. | Alum. 1100-0 | .004 | 22½ | As rec'd. | 25,906 | 41.5 | |
| 2. | " " | " | " | " " | 30,000 | 20.9 | |
| 3. | " " | " | " | " " | 33,708 | 50.5 | |
| 4. | " " | " | " | " " | 33,898 | 36.8 | |
| 5. | BeCu, 25 | .002 | 17 | 340 | 30,000 | 29.8 | |
| 6. | " " | " | 21 | 310 | 30,000 | 34.8 | |
| 7. | " " | " | 27 | 380 | 30,000 | 50.7 | |
| 8. | Brass, 70/30 | .002 | 24 | 380 | 30,000 | 44.8 | |
| 9. | Alum. 1100-0 | .004 | 22½ | 180 | 34,286 | 27.3 | |
| 10. | " " | " | " | " | 33,333 | 35.2 | |
| 3/16/82 | | | | | | | |
| 11. | Alum. 1100-0 | .004 | 22½ | 180 | 25,000 | - | Partially unwrapped |
| 12. | " " | " | " | " | 30,000 | 31.8 | |
| 13. | " " | " | " | " | 33,776 | 15.0 | |
| 14. | " | " | " | " | 25,000 | 34.0 | |
| 15. | " " | " | " | " | 33,333 | 36.4 | |
| 16. | Lead | .0025 | 15 | 80 | 30,612 | 22.7 | |
| 17. | " | .0012 | 28 | 20 | 30,000 | 42.1 | |
| 18. | Aluminum | .002 | 30 | 250 | 30,303 | 53.7 | |
| 19. | Brass, 70/30 | .004 | 26 | 570 | 30,000 | 33.8 | |
| 20. | Cu, OFHC | .0015 | 22 | 280 | 30,612 | 59.5 | |
| 21. | " " | " | 16 | 380 | 33,784 | 40.2 | |
| 22. | Aluminum, 1145 | .0012 | 23 | 280 | 30,000 | - | Partially unwrapped |
| 23. | " " | " | 22 | 340 | 33,708 | - | " " |

TABLE 1 TEST DATA

| NO. | MATERIAL | THICKNESS INCHES | LENGTH INCHES | TENSION GRAMS | SPINNER RPM | TIME MILLISEC'S. | REMARKS |
|---|---|---|---|---|---|---|---|
| 4/5/82 | | | | | | | |
| 24. | Alum. 1100-0 | .004 | 22½ | 180 | 30,000 | 33.1 | |
| 25. | Lead | .002 | 27 | 80 | 26,000 | 3.6 | Time appears questionable |
| 26. | Aluminum, 1145 | .0012 | 13 | 140 | 33,000 | - | Only 4" unwrapped |
| 27. | " " | " | 28 | 140 | 29,000 | - | Only 13½" unwrapped |
| 28. | Alum. 1100-0 | .004 | 12 | 180 | 27,000 | 22.2 | |
| 29. | BeCu, 25 | .002 | 17 | 340 | 33,000 | 34.1 | |
| 30. | Lead | .002 | 21 | 80 | 31,600 | 51.7 | |
| 31. | Alum. 1100-0 | .004 | 17 | 180 | 20,000 | 39.2 | |
| 32. | " " | " | 22½ | 180 | 27,000 | 37.7 | |
| 33. | Lead | .002 | 14 | 80 | 22,000 | 9.8 | Time appears questionable |
| 34. | Brass, 70/30 | .002 | 39 | 250 | 30,000 | 63.5 | |
| 35. | Aluminum, 1145 | .0012 | 18 | 140 | 33,000 | - | Only 13" unwrapped |
| 36. | " " | " | 31 | 140 | 29,000 | - | Only 14½" unwrapped |
| 37. | Alum. 1100-0 | .004 | 22½ | 140 | 30,000 | 29.8 | |
| 5/10/82 | | | | | | | |
| 38. | BeCu, 25 | .002 | 22 | 240 | - | - | Unwound prematurely |
| 39. | Cu, OFHC | .0015 | 18 | 450 | 20,000 | - | Did not unwind |
| 40. | Brass, 70/30 | .004 | 12 | 490 | - | - | Unwound prematurely |
| 41. | " " | " | 27 | 300 | 31,100 | 35.7 | |
| 42. | " " | " | 14 | 260 | 24,000 | 29.5 | |
| 43. | " " | " | 12 | 440 | 26,000 | 33.7 | |
| 44. | BeCu, 25 | .002 | 10 | 500 | - | - | Unwound prematurely |
| 45. | Brass, 70/30 | .002 | 30 | 230 | 28,000 | 149.6 | |
| 46. | Cu, OFHC | .0015 | 14 | 150 | 30,000 | 53.1 | |
| 47. | BeCu, 25 | .002 | 21 | 270 | 29,000 | 23.0 | |
| 48. | Brass, 70/30 | .004 | 11 | 180 | 28,000 | 19.9 | |
| 49. | Brass " | .004 | 23 | 320 | 26,000 | 29.7 | |
| 50. | Cu, OFHC | .0015 | 30 | 490 | 25,000 | 108.1 | |
| 51. | Brass, 70/30 | .004 | 26 | 240 | 21,000 | 39.9 | |
| 52. | " " | " | 15 | 430 | 31,000 | 30.5 | |
| 53. | " " | .002 | 19 | 340 | 30,000 | 47.4 | |
| 54. | BeCu, 25 | .002 | 23 | 260 | 31,900 | 30.2 | |
| 55. | " " | " | 29 | 360 | - | - | Unwound prematurely |

TABLE 1 TEST DATA

| NO. | MATERIAL | THICKNESS INCHES | LENGTH INCHES | TENSION GRAMS | SPINNER RPM | TIME MILLISEC'S. | REMARKS |
|---|---|---|---|---|---|---|---|
| 5/10/82 | | | | | | | |
| 56. | Alum. 1100-0 | .004 | 10 | 200 | 25,000 | 22.1 | |
| 57. | " " | " | 15 | 180 | 30,000 | 19.4 | |
| 58. | Brass, 70/30 | " | 27 | 300 | 31,600 | 45.9 | |
| 59. | " " | " | 27 | 300 | 31,600 | 35.0 | |
| 60. | " " | .002 | 30 | 230 | 28,000 | 75.5 | |
| 61. | BeCu, 25 | .002 | 29 | 360 | 24,000 | 39.2 | |
| 62. | Cu, OFHC | .0015 | 16½ | 450 | 25,000 | 54.3 | Unit No. 39 with 1½" remove |
| 63. | Alum. 1100-0 | .004 | 22½ | 180 | 30,000 | 32.2 | |
| 64. | " " | " | " | " | 30,000 | 38.1 | |
| 65. | " " | " | 16 | " | 25,000 | 34.5 | |
| 66. | " " | " | " | " | 20,000 | 51.0 | |
| 67. | " " | " | " | " | 18,000 | 60.0 | |
| 68. | " " | " | " | " | 17,000 | 62.9 | |
| 69. | " " | " | " | " | 15,000 | - | Partially unwrapped |
| 70. | " " | " | 22½ | " | 32,400 | 24.8 | |



TABLE 1 TEST DATA

FIG. 6 UNWINDING RATE MEASURED FROM HIGH SPEED FILMS

.004 Aluminum, 22½" Long, Approx. 25,000 RPM

Film Speed Approx. 5,000 Frames/Sec.

- Ribbon No. 2 Wound in Direction of Rotation
- Ribbons 1,3,4 Wound Opposite to Direction of Rotation

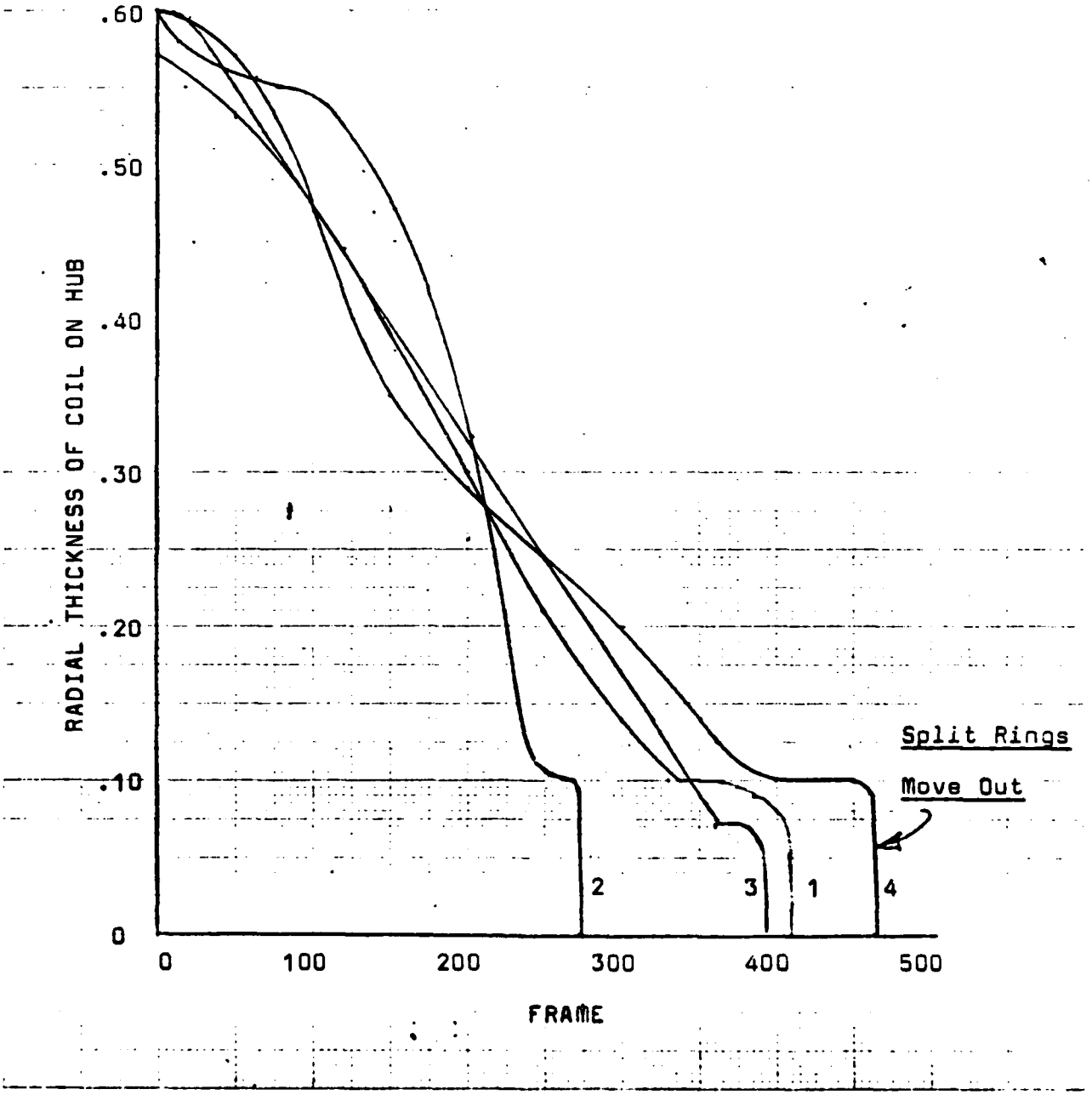

different unwinding history. The films of this event showed many coils existing in the space between the hub and the outer cavity. In contrast, the other ribbons showed only one coil at a time being transferred to the outer cavity wall.

(4) The shape of the bridge was a flat spiral, with no noticeable changes in shape as unwinding proceeded.

The observations made above were used as justification for the pseudo-stationary models developed in Section 4 of this report.

None of the six assemblies using .0012 inch (.0305mm) thick aluminum unwrapped completely, although three of the assemblies were spun at 33,000 rpm. Evidently there is not sufficient force generated at the free end of such a thin ribbon to sustain the unwrapping function.

To comment on the relative advantages of the materials used in the test program, it appears that the selection of 1100-0 aluminum for the ribbon unwinder assemblies used in the XM579 fuze was a good selection. It is inexpensive, relatively easy to wind, and does not require annealing.

## 3. MULTIVARIATE REGRESSION ANALYSIS BY ALN METHOD

### 3.1 Discussion of the Data

The objective of the work presented in this report was to obtain an empirical model that relates the ribbon unwinding time to the experimental and material-dependent parameters. The method for obtaining this model was the application of the Adaptive Learning Network (ALN) method to data collected for the present study, as well as data collected in other tests.

The ALN method is an empirically-based modeling procedure. This procedure is presented in detail in Appendix A. The advantage of this technique is the ability to obtain highly nonlinear and multidimensional models. It should be noted, however, that only that model complexity supported by the data is obtained. The ALN method does not force nonlinearity or multidimensionality into the models.

The data obtained for the present study were obtained using a spinner setup. That is, a ribbon was wound around the hub of a shell, the shell spun, and the time required for the ribbon to unwind measured. The factors that were varied were the material the ribbon was made of, its length, thickness, the spin rate, and the winding tension. The ribbons were constructed of five different materials: aluminum, beryllium-copper, brass, lead, and copper. The lengths of the ribbons varied from 10 to 30 inches, and their thicknesses varies from 1.2 to 4 mils. The winding loads were varied from 20.2 to 570 grams, and the spin rates varies from 15,000 to 33,898 rpm. A complete list of the data obtained for this study has been presented in Table 1.

Data similar in nature to the present data have been obtained in other spinner and firing tests(Ref.1,2). See Table 2.

TABLE 2 RIBBON UNWINDING DATA FROM OTHER TESTS

| TEST | CONDITION | LINER THICK. | $R_0$ IN. | $R_1$ IN. | MATL. | n in. | L in. | RPM | NO. TESTS | MEAN MS | SIGMA |
|---|---|---|---|---|---|---|---|---|---|---|---|
| Bulova | 70°F | .020 | .335 | .100 | Alum. | .004 | 24 | 34,500 | 1 | 50 | |
| | " | " | " | " | " | " | " | " | 1 | 60 | |
| Spinner | 160°F | " | " | " | " | " | " | " | 1 | 52 | |
| | " | " | " | " | " | " | " | " | 1 | 53 | |
| | " | " | " | " | " | " | " | " | 1 | 46 | |
| | -10°F | " | " | " | " | " | " | " | 1 | 50 | |
| Frost | -35/-20°F | " | " | " | " | " | " | " | 1 | 100 | |
| | " | " | " | " | " | " | " | " | 1 | 74 | |
| | 70°F | " | " | " | " | " | " | 29,000 | 6 | 48.6 | 1.1 |
| | " | " | " | " | " | " | " | 34,000 | 24 | 54.8 | 8.3 |
| | " | " | " | " | " | " | " | 36,000 | 9 | 46.6 | 7.0 |
| | " | - | " | .125 | " | .006 | 5 | 34,000 | 1 | 6 | |
| | " | - | " | " | " | " | 5 | " | 1 | 6 | |
| | " | - | " | .0625 | G.M. | .003 | 10 | " | 1 | 12 | |
| | " | - | " | " | " | " | 10 | " | 1 | 11 | |
| | " | - | " | " | Al+GM | .013 | 6 | " | 1 | 7 | |
| | " | - | " | .100 | Alum. | .006 | 11 | " | 1 | 14 | |
| | " | - | " | " | " | " | 11 | " | 1 | 16 | |
| | " | - | " | " | " | " | 11 | " | 1 | 16 | |
| | " | - | " | " | G.M. | " | 11 | " | 1 | 15 | |
| | " | - | " | " | " | " | 11 | " | 1 | 14 | |
| | " | - | " | " | " | " | 11 | " | 1 | 14 | |
| | " | - | " | " | Alum. | .004 | 24 | " | 1 | 37 | |
| | " | - | " | " | " | " | " | " | 1 | 37 | |
| | " | - | " | " | " | " | " | " | 1 | 31 | |
| | " | - | " | " | G.M. | .003 | 11 | " | 1 | 15 | |
| | " | .020 | " | " | Alum. | .004 | 12 | " | 11 | 27 | 8 |
| | " | .015 | " | " | " | " | 15 | " | 9 | 39 | 13 |
| | " | .020 | " | " | " | " | 24 | " | 11 | 41 | 5 |
| | " | .030 | " | " | " | " | 24 | " | 7 | 51 | 10 |
| | " | .020 | " | " | " | " | 25 | " | 9 | 66 | 16 |
| | " | .020 | " | " | " | " | 24 | " | 7 | 50 | 14 |
| | " | .020 | " | " | " | " | 24 | " | 10 | 42 | 8 |
| 20mm | " | - | .217 | .074 | Brass | " | 9 | 75,000 | 1 | 10.9 | |
| Firings | " | - | " | .068 | " | " | 8 | " | 1 | 9.4 | |
| | " | - | " | .068 | " | " | 6 | " | 1 | 8.3 | |
| | " | - | " | .068 | " | " | 5 | " | 1 | 7.1 | |

Review of the data in Tables 1 and 2 reveals a number of interesting factors. First, the data in Table 1 shows there were a number of experimental trials where the ribbon did not unwind completely but where, in other trials under identical or near-identical conditions, the ribbon did unwind completely. For example, trials 11 and 14 in Table 1 represent such a case. The second observation is that the data demonstrate a certain variability, the lack of unwinding completely when they should and nearly identical trials having times varying by a factor of two (eg. trials 10 and 13). A third observation has to do with the relationship between spin rate and unwinding time. Figure 7 displays a plot of the unwinding time vs. spin rate for trials involving aluminum of 4-mil thickness and 22.5 inches length. A decrease in the unwinding time with increasing spin rate is indicated but the variance of the data is large enough to be consistent with no dependence of one on the other. (The line shown results from a least squares fit to the data). These observations are an indication that there are experimental difficulties with obtaining reproducible results.

Experimental measurements made under "identical" conditions exhibit variability in their values due to random fluctuations in the experimental process. The data in Table 2, taken from other spinner and firing tests, demonstrate variability (for the spinner data) that is inconsistent with random fluctuations. The data listed on lines 10 and 29 were nominally taken under identical experimental conditions. The first gave a mean time of 54.8 ms with a standard deviation of 8.3 ms for 24 measurements. The second resulted in a mean time of 41 ms with a 5 ms standard deviation for 11 measurements. These two sets of measurements can be tested to determine if the measured differences resulted from random fluctuations. The "T"

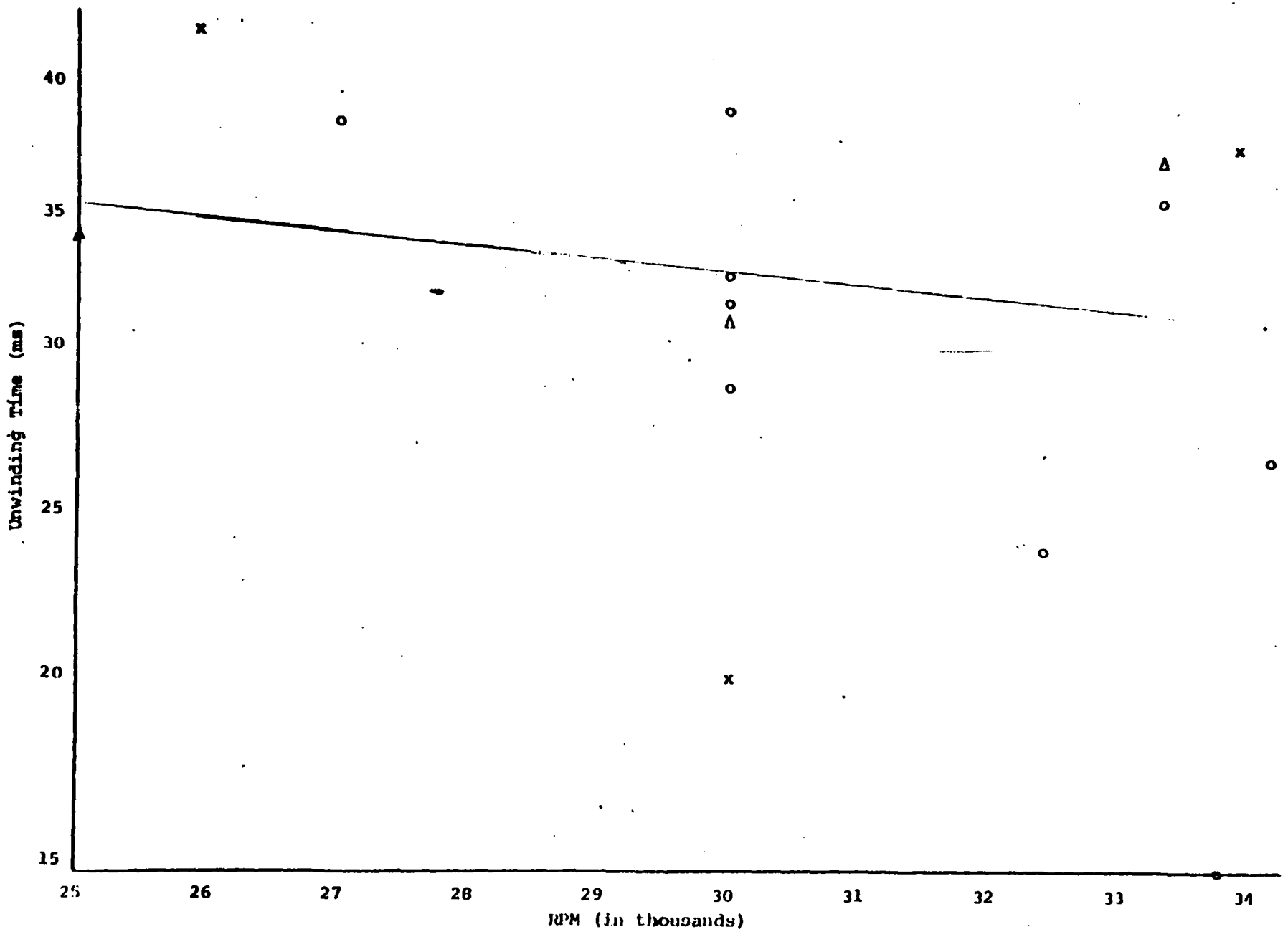


FIGURE 7 UNWINDING TIME VS. RPM

statistic for testing the equality of the means of two samples is used (Ref.5):

$$T = \frac{\left(\frac{nm}{n+m}\right)^{\frac{1}{2}}(\bar{x}-\bar{y})}{\left(\frac{nS_x^2+mS_y^2}{n+m-2}\right)^{\frac{1}{2}}} \qquad \text{Eq. (1)}$$

where $\bar{x}$ and $\bar{y}$ are the means of the two samples, $S_x$ and $S_y$, their standard deviations, and $n$ and $m$ the number of samples of x and y, respectively. For the data given above, T=4.96. From the tables for T distributions, the probability of obtaining a value of T at least as large as 4,96, for $n+m-2 = 33$ degrees of freedom, is less than 0.0005. The conclusion to be drawn from this is that the different results obtained for the two samples did not occur due to random fluctuations, but must be due to uncontrolled or unrecorded variables. This set of data (Table 2) is therefore of questionable value for modeling purposes and was not used in obtaining any of the results presented below.

## 3.2 Adaptive Learning Network Model

The ALN modeling procedure involves identifying candidate independent variables that are used as inputs to the model to predict the sought-after quantity, in this case, the ribbon unwinding time. The list of candidate features should include, ideally, all the variables that could conceivably affect the quantity being modeled. The values of the independent variables, aling with the values of the quantity being modeled, are the input data to an Adaptronics, Inc. proprietary model synthesis program.

This program considers all the candidate independent variables in different combinations and chooses that set of combinations that best (in the statistical sense) predict the dependent variable. A complete description of this process is given in Appendix A.

The independent variables for the present data included both test parameters and material-dependent parameters, and are listed in Table 3.

TABLE 3 CANDIDATE VARIABLES

| Independent Variables | Symbol |
|---|---|
| 1. Spinner RPM | R |
| 2. Material Density | $\mu$ |
| 3. Young's Modulus | Y |
| 4. Longitudinal Wave Velocity | $V_L$ |
| 5. Shear Wave Velocity | $V_S$ |
| 6. Thickness | T |
| 7. Length | L |
| 8. Winding Load | W |

Values of the independent variables in Table 3 are given either in Table 1 or in Table 4, below.

TABLE 4 VALUES FOR INDEPENDENT VARIABLES

| Material | Density, lb/cu.in. | Young's Modulus 1000 psi | Sound Velocity, km/sec Longitudinal | Shear |
|---|---|---|---|---|
| Aluminum | 0.097 | 10,300 | 6.3 | 3.1 |
| Brass | 0.300 | 16,000 | 4.4 | 2.1 |
| Be-Cu | 0.300 | 17,000 | - | - |
| Copper | 0.320 | 17,000 | 4.7 | 2.3 |
| Lead | 0.410 | 2,000 | 2.2 | 0.7 |

Using the data in Tables 1 and 4 as inputs to the ALN model synthesizing program the following model was obtained for predicting the unwinding time in milliseconds:

$$t = 16.096\,\bar{t} + 39.574 \qquad \text{Eq. (2)}$$

$$\bar{t} = -.00001 + .90886A + .75419B + .77141AB - .25692B^2 \qquad \text{Eq. (3)}$$

$$A = .53317/\bar{R} - .48854\bar{T} + .41874\bar{L} \qquad \text{Eq. (4)}$$

$$B = -1.80102 + 5.1832\bar{\mu} - 5.66211\bar{\gamma} + 4.89211\bar{\mu}\bar{\gamma} \qquad \text{Eq. (5)}$$

where

$$1/\bar{R} = (1/R - .36016\times10^{-4})/.64743\times10^{-5} \qquad \text{Eq. (6)}$$

$$\bar{T} = (T - .3128\times10^{-2})/.10877\times10^{-2} \qquad \text{Eq. (7)}$$

$$\bar{L} = (L - 21.095)/5.8356 \qquad \text{Eq. (8)}$$

$$\bar{\mu} = (\mu - .22334)/.11044 \qquad \text{Eq. (9)}$$

$$\bar{\gamma} = (\gamma - 13{,}006)/4{,}084.3 \qquad \text{Eq. (10)}$$

The model that resulted indicates that the reciprocal of the RPM, the thickness of the ribbon and its length all enter linearly into the model. The density and Young's Modulus enter nonlinearly. This model is the best one that can be obtained using the inputs described above.

The output of the ALN model synthesizing program is such that many "intermediate models" are also produced. One such model that gave good results (but not as good as the complete model presented above) was one that used A from Eq. 4 above in place of $\bar{t}$ in Eq. 2. This second model is presented only because it is simpler than the above model and yet gave good results.

Table 5 lists the predicted unwinding times for the measurement where the ribbons did not unwind completely. These values were obtained using the complete model given above.

TABLE 5 PREDICTED UNWINDING TIMES FOR TRIALS WHICH DID NOT UNWIND

| Test No. | Material | Time, ms |
|---|---|---|
| 11 | Aluminum | 36.8 |
| 22 | Aluminum | 45.2 |
| 23 | Aluminum | 41.0 |
| 25 | Lead | 54.5 |
| 26 | Aluminum | 34.3 |
| 27 | Aluminum | 50.3 |
| 33 | Lead | 49.5 |
| 35 | Aluminum | 38.3 |
| 36 | Aluminum | 52.7 |
| 39 | Copper | 27.8 |
| 69 | Aluminum | 56.3 |

Fig. 8 shows a computer-generated plot of the difference between the predicted and observed value of the unwinding time vs. the observed value. The model is the complete model presented above. The straight line shown results from a linear least squares fit to the data. This plot shows that the synthesized model tends to predict unwinding times that are too large for small unwinding times and too small for the longer times. The small slope and the variability of the data about the line may make the data statistically consistent with zero slope. Testing this, however, would require knowledge (which is unavailable) of the experimental uncertainties.

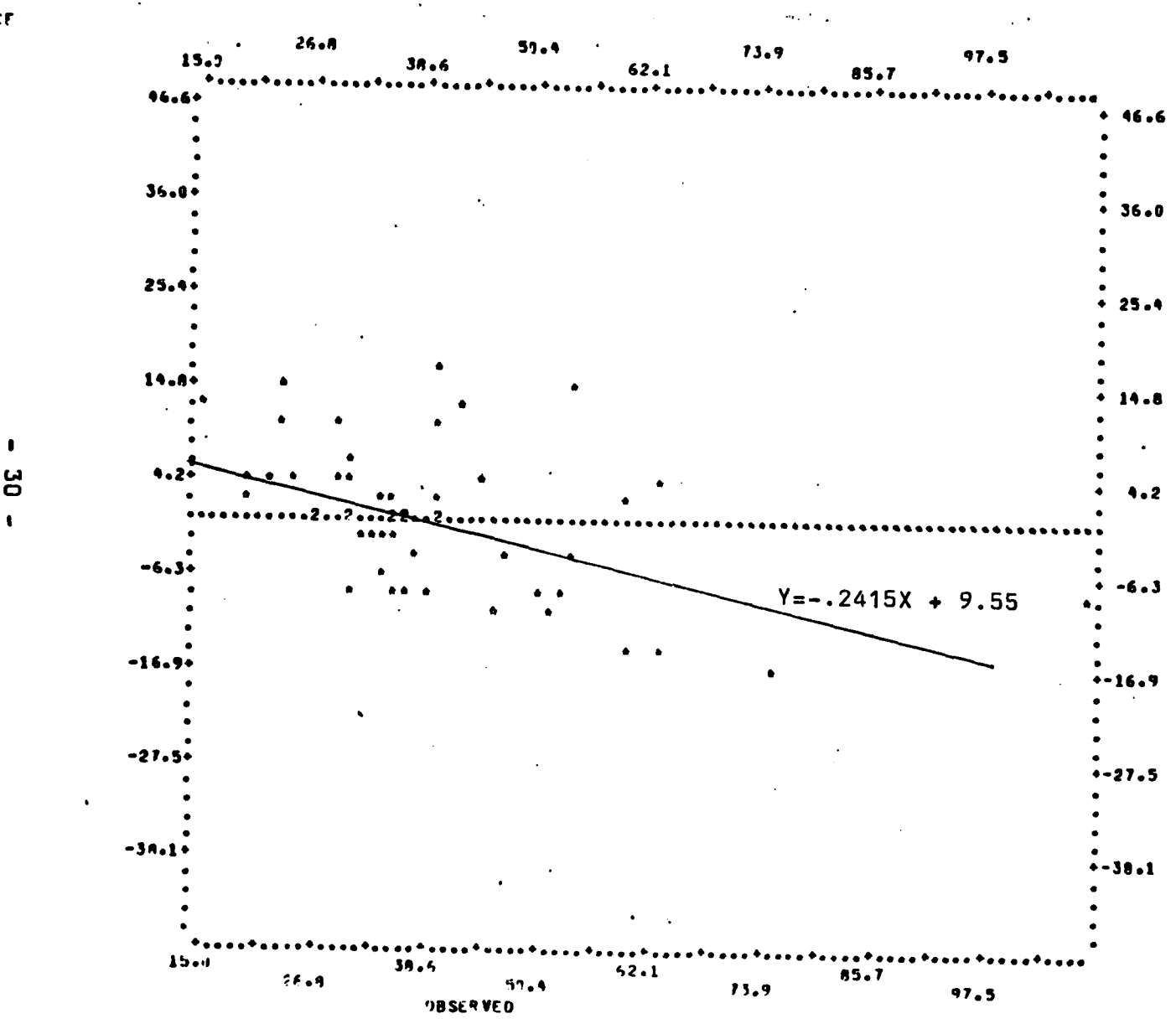


FIG. 8 DIFFERENCE OF PREDICTED AND OBSERVED VALUES VS. THE OBSERVED VALUES

## 3.3 Discussion of Results

The experimental and modeling results presented above display a number of interesting features. First, the ALN model for predicting unwinding time and which resulted from fitting to the data, found that the data did not support the inclusion in the model of a "cross term" between length and reciprocal spin rate. On simple physical grounds the unwinding time of a ribbon is expected to be proportional to the length divided by the velocity of unwinding. The fact that such a term does not appear indicates only that the present data does not support its inclusion.

The second observation concerns the results in Table 5. This table presents the unwrapping time predicted by the ALN model for the experimental trials in which the ribbons did not completely unwind. The predicted unwinding times indicate that all the ribbons should have unwound completely.

The third observation concerns Fig. 8. The results in this figure suggest that there is one or more experimental factors which are not accounted for in the ALN model and which result in the model predicting too long an unwinding time for short unwinding times and too short a time for the longer times. Note that this observation is based on an assumption that the observed slope to the data is statistically inconsistent with zero. If the slope is statistically consistent with zero then the results shown in Fig. 8 could have resulted from normal random fluctuations in experimental processes. In an attempt to determine if the missing factor was material-related the plot shown in Fig. 8 was redone, highlighting the different materials. No correlation with ribbon material was evident.

The conclusions that can be drawn from the present data analysis are the following. First, the ALN model that was obtained from fitting to the experimental data in Table 1 identified five variables as being important for predicting ribbon unwinding times. Those variables were: ribbon length, thickness, density, Young's modulus, and the reciprocal of the spin rate. Three of these (1/R, T, and L) entered into the model linearly and the other two nonlinearly.

The second conclusion is the present modeling results suggest that there is one or more unspecified experimental factors that result in the synthesized model predicting times which are too long for small unwinding times (less than 40 ms) and too short for longer unwinding times.

The third conclusion is that the present data displays a large variability. For approximately 15 percent of the experimental trials the ribbons did not unwind completely. The other data and the modeling results indicate that the ribbons should have unwound completely.

The fourth conclusion is that the data from other spinner tests, listed in Table 2, cannot be reliably used for modeling purposes. Nominally identical sets of measurements gave results which are inconsistent and could not have resulted from random fluctuations. The present analysis indicates that future work in the area of ribbon unwinders should first concentrate on determining the experimental factors involved in obtaining reproducible results.

## 4. ANALYTICAL MODELS OF UNWINDER DYNAMICS

### 4.1 The Straight Bridge Model

Fig. 9 shows two possible configurations of the bridge, or ribbon moving in the space between the coil on the hub and the coil deposited inside the cavity. The dashed ribbon shape resembles the shape observed by high speed photography, but the straight-line shape is more convenient for approximate analysis. A radial force $F_p$ is shown inside the coil to represent the centrifugal force exerted by a pin, as in the XM579 fuze, or by the split hub segments employed in this test program. The forces on a particle with mass m moving in the rotating field with relative radial velocity $V_r$ and relative tangential velocity $V_t$ are as follows:

Radial force, $$F_r = m(\omega^2 r + V_t^2/r + 2\omega V_t) \qquad \text{Eq. (11)}$$

Coriolis force, $$F_c = 2m\omega V_r \qquad \text{Eq. (12)}$$

If the ribbon is assumed to have no bending stiffness, the only other forces on the bridge will be cavity friction force $f_c$, hub friction force $f_h$, and inertial reactions if the hub and/or bridge mass are being accelerated.

Using Eq.11 and Eq.12, the dynamics of unwinding could be studied from the time the free end of the coil starts to unwind from the hub until the entire coil has been transferred to the cavity wall. The bridge shape (which could change throughout the unwinding process) and the motion of each ribbon particle could be calculated

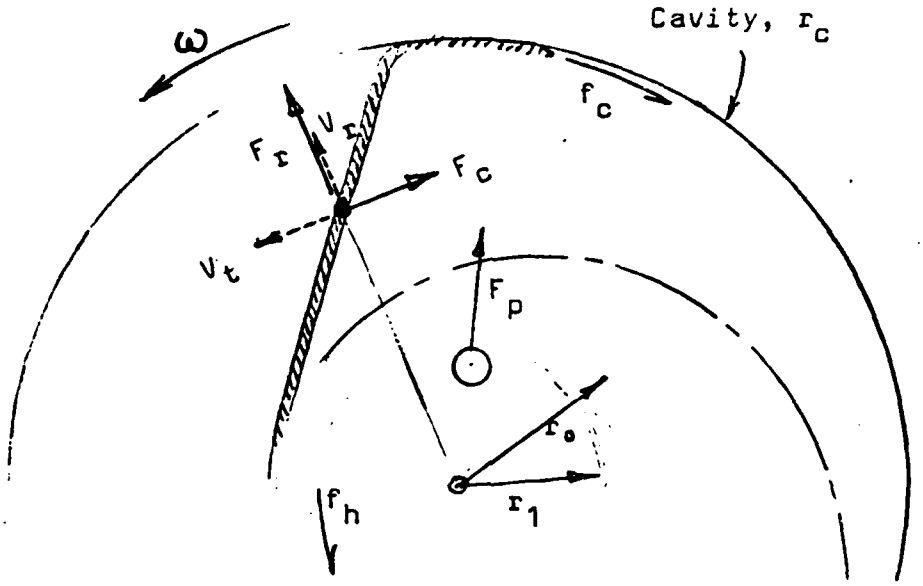


FIG. 9 RELATIVE VELOCITIES AND FORCES, STRAIGHT BRIDGE MODEL

From Eq.11, Eq.12, and Newton's laws relating forces to changes in $V_r$ and $V_t$. Although this approach would be extremely valuable in revealing the effects of material density, bending stiffness and friction, it is well beyond the scope of the present program of analysis. Instead, the multivariate regression analysis of experimental data is relied upon to reveal the influence of these parameters, and the analysis is restricted to the more approximate approach of evaluating ribbon dynamics with an assumed bridge shape.

It was observed experimentally that ribbon unwinding velocity was fairly constant, and the bridge shape remained fairly constant, all throughout the unwinding process. This implies a pseudo-stationary process with no acceleration

of the hub. Also, since the bridge shape is stationary in the rotating coordinate system, there are no net accelerations on the ribbon particles beyond those required to maintain the bridge in that configuration. These assumptions permit the unwinding dynamics to be analyzed from a rather simplified viewpoint, namely, to determine what ribbon unwinding velocity will produce centrifugal and Coriolis accelerations that maintain the assumed (constant) bridge shape. This approach is used to analyze the straight bridge model (and also the standing wave model) as follows.

Fig. 10 shows the straight bridge model with mass concentrated at the midpoint of the bridge, in its initial position and then after ribbon length $\theta_u r_c$ has been deposited on the cavity wall. The point of tangency at the hub moves through angle $\theta_u$. In order for the length of the bridge to remain unchanged, the hub must rotate through angle $\theta_h$ as follows:

$$r\theta_h + r\theta_u = r_c\theta_u$$

$$\theta_h/\theta_u = r_c/r - 1 \qquad \text{Eq. (13)}$$

The bridge's center of gravity moves from its initial position at $AD = \frac{1}{2}(r_c^2 - r^2)^{\frac{1}{2}}$ to $BC = AD - r_c\theta_u$. Its radial distance is now increased to $\left[r^2+(2AD-BC)2\right]^{\frac{1}{2}} = \left[\frac{3}{4}r^2+\frac{1}{4}r_c^2+r_c\theta_u(r_c^2-r^2)^{\frac{1}{2}}+r_c^2\theta_u^2\right]^{\frac{1}{2}}$. For small values of $\theta_u$ this expression reduces to $(\frac{3}{4}r^2+\frac{1}{4}r_c^2)^{\frac{1}{2}} + \dfrac{r_c\theta_u(r_c^2-r^2)^{\frac{1}{2}}}{2(\frac{3}{4}r^2+\frac{1}{4}r_c^2)^{\frac{1}{2}}}$

The change in radial distance from its original radius of $r_2 = \left[r^2+\frac{1}{4}(r_c^2-r^2)\right]^{\frac{1}{2}}$ is as follows:

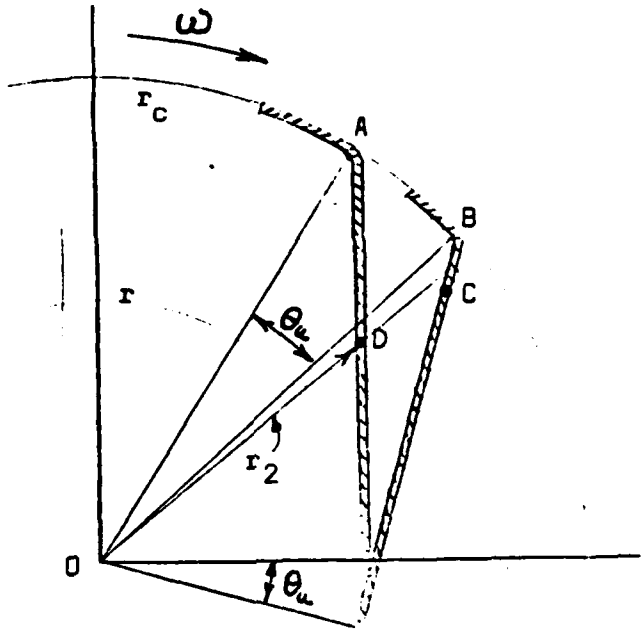


FIG. 10 MOTION OF BRIDGE WITHOUT SLIPPAGE AT CAVITY

$$\Delta r = r_c\theta_u \left(\frac{r_c^2 - r^2}{r_c^2 + 3r^2}\right)^{\frac{1}{2}}$$

$$\frac{\Delta r}{r_c\theta_u} = \left(\frac{r_c^2/r^2 - 1}{r_c^2/r^2 + 3}\right)^{\frac{1}{2}} \qquad \text{Eq. (14)}$$

The angle of rotation of the radius vector OD to OC is equal to $\tan^{-1}AD/r - \tan^{-1}\frac{2AD-BC}{r} + \theta_u$. Since $\tan^{-1}x - \tan^{-1}y = (x-y)/(1+xy)$, the angle of rotation is equal to:

$$\theta_u - \frac{r(AD - BC)}{r^2+2(AD)^2-(AD)(BC)} = \theta_u - \frac{r(r_c\theta_u)}{r^2+\frac{1}{2}(r_c^2-r^2)-\frac{1}{2}(r_c^2-r^2)^{\frac{1}{2}}\left[\frac{1}{2}(r_c^2-r^2)^{\frac{1}{2}}-r_c\theta_u\right]}$$

$$\approx \theta_u\left(\frac{\frac{3}{4}r^2+\frac{1}{4}r_c^2-rr_c}{\frac{3}{4}r^2+\frac{1}{4}r_c^2}\right).$$ Tangential motion is obtained by

multiplying the angular change $\Delta\theta$ by radial distance $r_2$:

$$r_2\Delta\theta = \theta_u \frac{\frac{3}{4}r^2+\frac{1}{4}r_c^2-rr_c}{(\frac{3}{4}r^2+\frac{1}{4}r_c^2)^{\frac{1}{2}}} = \theta_u \frac{(r_c-r)(r_c-3r)}{2(3r^2+r_c^2)^{\frac{1}{2}}}$$

$$\frac{r_2\Delta\theta}{r_c\theta_u} = \frac{(r_c/r-1)(r_c/r-3)}{(2r_c/r)(3+r_c^2/r^2)^{\frac{1}{2}}} \qquad \text{Eq. (15)}$$

Radial motion $\Delta r/r_c\theta_u$ and tangential motion $r_2\Delta\theta/r_c\theta_u$ are plotted in Fig. 11 vs. $r_c/r$.

Radial force $F_r$ and tangential force (or Coriolis force) $F_c$ are shown in Fig.9. Tensile force T along the ribbon will be as follows:

$$T = F_r\frac{(r_c^2-r^2)^{\frac{1}{2}}}{(r_c^2+3r^2)^{\frac{1}{2}}} + F_c\frac{2r}{(r_c^2+3r^2)^{\frac{1}{2}}} \qquad \text{Eq. (16)}$$

where $F_r$ and $F_t$ are given in Eq.11 and Eq.12 in terms of radial velocity $V_r$ and tangential velocity $V_t$.

The net tangential force is equal to $F_c - T\frac{2r}{(r_c^2+3r^2)^{\frac{1}{2}}}$ and it will be equal to zero if the bridge shape remains constant as the ribbon unwinds. Therefore:

$$F_c = T\frac{2r}{(r_c^2+3r^2)^{\frac{1}{2}}} = F_r\frac{2r(r_c^2-r^2)^{\frac{1}{2}}}{(r_c^2+3r^2)} + F_c\frac{4r^2}{(r_c^2+3r^2)}$$

$$F_r/F_c = \frac{r_c^2-r^2}{2r(r_c^2-r^2)^{\frac{1}{2}}} = \tfrac{1}{2}(r_c^2/r^2-1)^{\frac{1}{2}} = \alpha \qquad \text{Eq. (17)}$$

FIG. 11 RADIAL AND TANGENTIAL MOTIONS

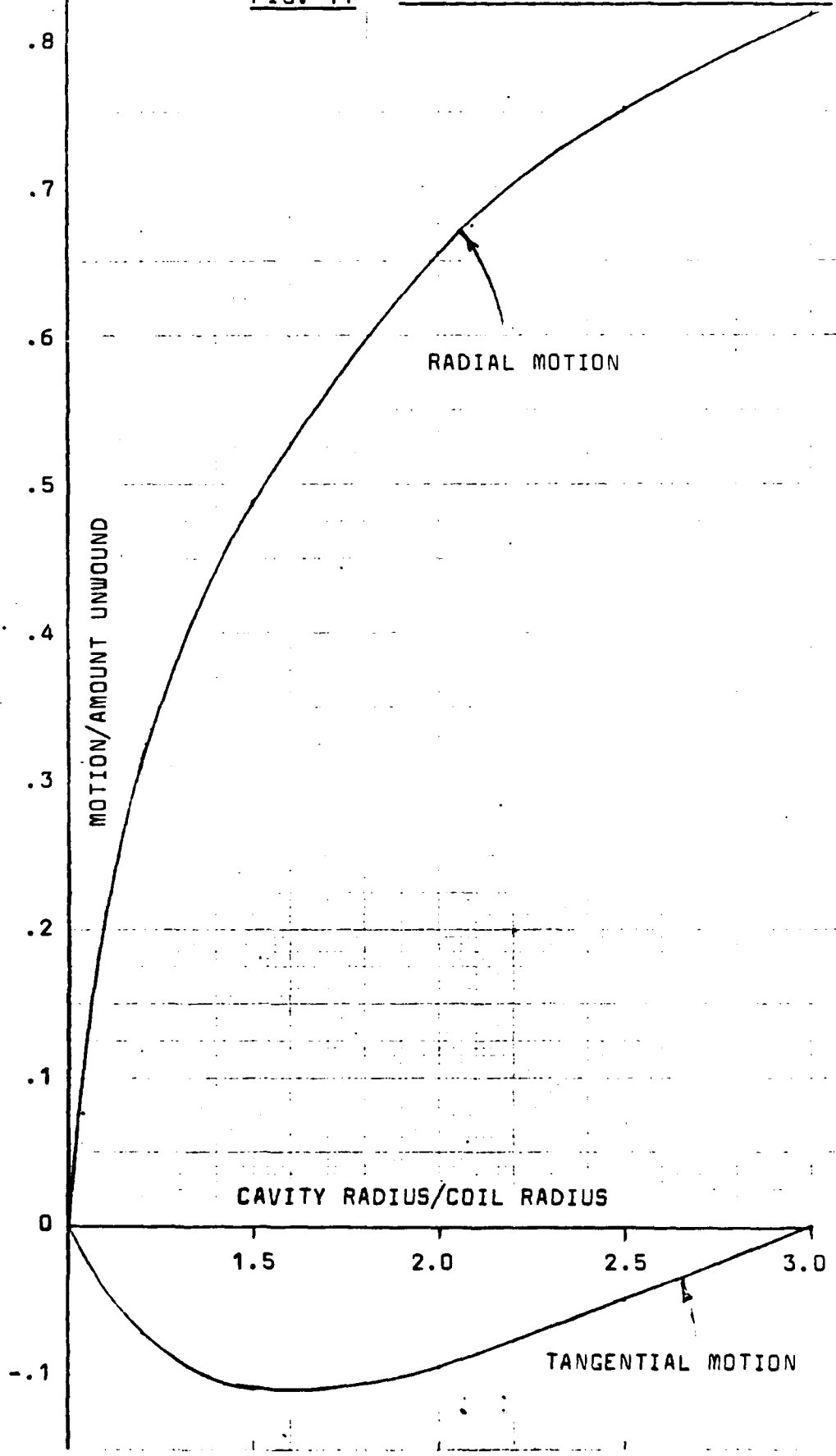

The same Eq. 17 is obtained if the net radial force is equated to zero. It is gratifying that the straight bridge model is consistent in this regard.

From Eq.11 and Eq.12:

$$F_r/F_c = \frac{\omega^2 r + V_t^2/r + 2\omega V_t}{2\omega V_r}$$

Combining this with Eq. 17:

$$2\alpha\omega V_r = \omega^2 r + V_t^2/r + 2\omega V_t \qquad \text{Eq. (18)}$$

$V_t$ and $V_r$ are also proportional to $r_2\Delta\theta$ and $\Delta r$, respectively. Combining these relationships with Eq. 14 and Eq.15:

$$V_r/V_t = \Delta r/r_2\Delta\theta = \frac{(2r_c/r)(r_c^2/r^2-1)^{\frac{1}{2}}}{(r_c/r-1)(r_c/r-3)} = \beta \qquad \text{Eq. (19)}$$

Combining Eq.18 and Eq.19:

$$V_t^2 + 2r\omega V_t(1-\alpha\beta) + \omega^2 r^2 = 0$$

$$2V_t = -2r\omega(1-\alpha\beta) - \left[4r^2\omega^2(1-\alpha\beta)^2 - 4\omega^2 r^2\right]^{\frac{1}{2}}$$

$$V_t/r\omega = \alpha\beta(1-2/\alpha\beta)^{\frac{1}{2}} + (1-\alpha\beta) \qquad \text{Eq. (20)}$$

where $\alpha\beta = (r_c/r)(r_c/r+1)/(r_c/r-3)$. To relate $V_t$ to unwinding rate dL/dt, note that Eq.15 relates tangential deflection to unwound length $r_c\theta_u$. Since $r_2\Delta\theta/V_t = r_c\theta_u/\dot{L}$:

$$\dot{L}/V_t = r_c\theta_u/r_2\Delta\theta \qquad \text{Eq. (21)}$$

Table 6 contains values of $\alpha\beta$, $V_t/r\omega$, $V_r/r\omega$, and $\dot{L}/r$ vs. $r_c/r$.

| $r_c/r$ | 1.0 | 1.2 | 1.5 | 2.0 | 2.5 | 2.9 |
|---|---|---|---|---|---|---|
| $\alpha\beta$ | -1.000 | -1.467 | -2.50 | -6.00 | -17.5 | -113 |
| $V_t/r\omega$ | .268 | .212 | .146 | .0719 | .0270 | .00438 |
| $V_r/r\omega$ | $\infty$ | .938 | .653 | .498 | .413 | .366 |
| $\dot{L}/r\omega$ | $\infty$ | 2.94 | 1.34 | .756 | .550 | .452 |

TABLE 6 UNWINDING RATE VS. $r_c/r$

Fig. 12 contains plots of $V_t$, $V_r$, and $\dot{L}$ vs. $r_c/r$ (plus velocity $V_s$ predicted by a standing wave model discussed in Section 4.2).

To calculate the unwinding time of any particular ribbon, $\dot{L}$ may be taken from Fig.12 for each value of $r_c/r$ as the ribbon unwinds. For a tightly wound ribbon, it may be shown that the length L remaining on the hub is as follows:

$$L = \pi(r^2 - r_1^2)/h \qquad \text{Eq. (22)}$$

where h is the ribbon thickness and $r_1$ is hub radius.

It may also be shown that the initial cavity radius $r_{co}$ is reduced approximately as follows:

$$r_c = r_{co} - h(L_o - L)/2\pi r_{co} \qquad \text{Eq. (23)}$$

Combining Eq.22 and Eq.23:

FIG. 12 VELOCITIES IN STRAIGHT BRIDGE MODEL

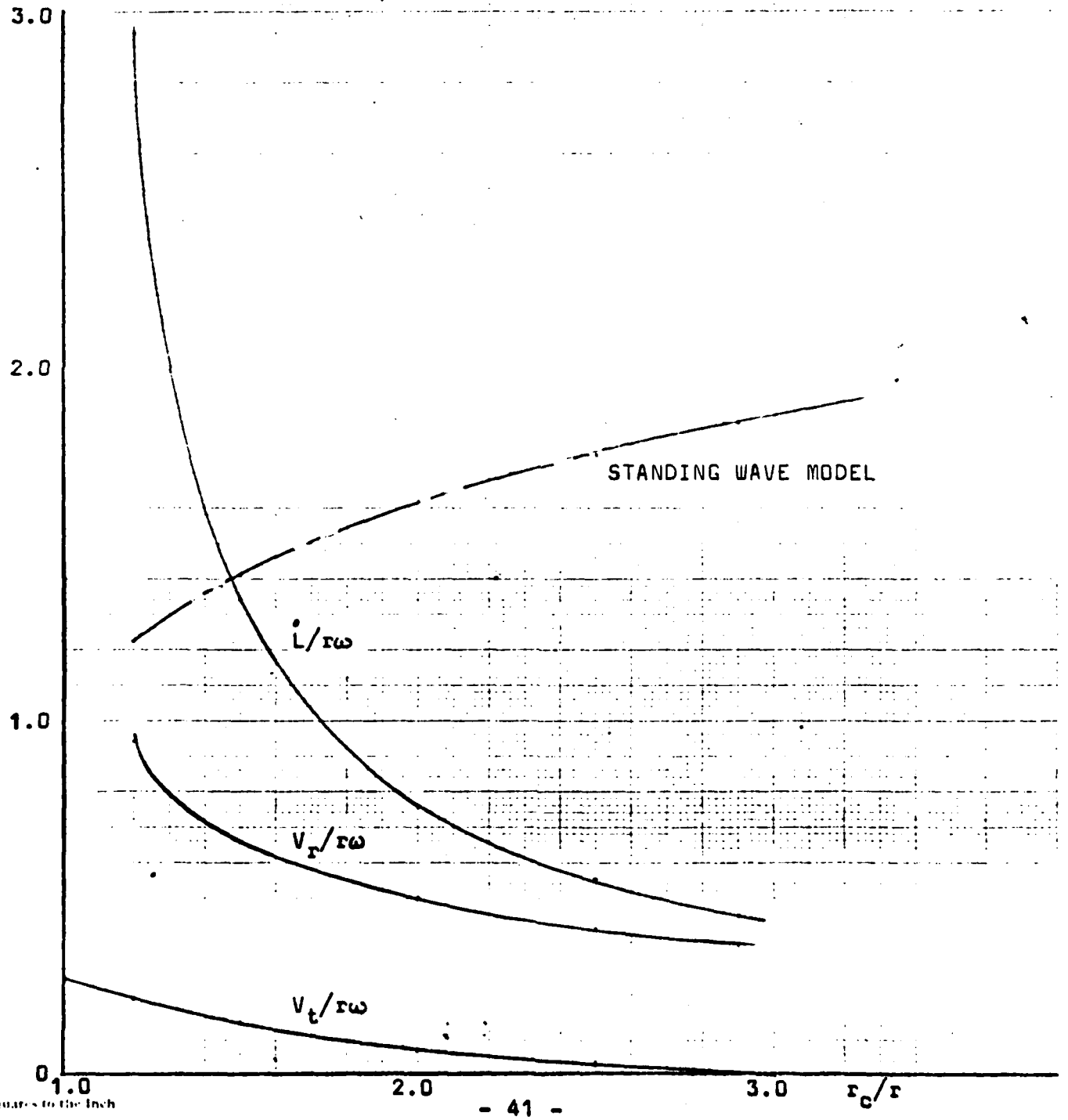

$$r_c/r = \frac{r_{co} - h(L_o - L)/2\pi r_{co}}{(hL/\pi + r_1^2)^{\frac{1}{2}}} \qquad \text{Eq. (24)}$$

A sample calculation is given in Table 7 for a 22.5 inch long aluminum ribbon with h =.004 inches tested at 30,000 rpm (3142 rad/sec) in the air spinner with $r_1$= .136 inches (outer radius of the split rings) and $r_{co}$=.342 inches.

| $\Delta L$, inches | 2.4 | 2.4 | 2.4 | 2.4 | 2.4 | 2.4 | 2.4 | 2.4 | 2.4 | 0.9 | |
|---|---|---|---|---|---|---|---|---|---|---|---|
| Mean L, in. | 21.3 | 18.9 | 16.5 | 14.1 | 11.7 | 9.3 | 6.9 | 4.5 | 2.1 | .45 | |
| r, in. (Eq.22) | .214 | .206 | .199 | .191 | .183 | .174 | .165 | .156 | .146 | .138 | |
| $r_c$ (Eq.23) | .340 | .335 | .331 | .326 | .322 | .317 | .313 | .308 | .304 | .301 | |
| $r_c/r$ | 1.59 | 1.63 | 1.66 | 1.71 | 1.76 | 1.82 | 1.90 | 1.97 | 2.08 | 2.18 | |
| $r\omega$, in/sec. | 672 | 648 | 624 | 600 | 574 | 547 | 519 | 489 | 457 | 434 | |
| $\dot{L}$, in/sec | 793 | 729 | 674 | 612 | 554 | 498 | 431 | 381 | 327 | 287 | |
| $\Delta t = \frac{\Delta L}{\dot{L}}$, ms | 3.03 | 3.29 | 3.56 | 3.92 | 4.33 | 4.82 | 5.57 | 6.29 | 7.35 | 3.14 | 45.3 ms |

TABLE 7 UNWINDING TIME OF 22.5 INCH RIBBON

Table 8 contains calculations of unwinding times of shorter ribbons with h = .004 inches and the same hub and cavity dimensions.

Tables 7 and 8 show that unwinding times decrease as $L_o$ decreases, but not nearly as much as if unwinding speed had remained constant. The 22.5 inch ribbon had an average unwinding speed of 515 in/sec, the 15 inch ribbon unwound at 397 in/sec, and the 10 inch ribbon unwound at 337 in/sec.

| $L_o$ | 15.0 | | | | | | 10.0 | | | |
|---|---|---|---|---|---|---|---|---|---|---|
| $\Delta L$ | 2.4 | 2.4 | 2.4 | 2.4 | 2.4 | 3.0 | 2.4 | 2.4 | 2.4 | 2.8 |
| Mean L, in. | 13.8 | 11.4 | 9.0 | 6.6 | 4.2 | 1.5 | 8.8 | 6.4 | 4.0 | 1.4 |
| r, in. | .190 | .182 | .173 | .164 | .154 | .143 | .172 | .163 | .154 | .142 |
| $r_c$, in. | .340 | .335 | .331 | .326 | .322 | .317 | .340 | .335 | .331 | .326 |
| $r_c/r$ | 1.79 | 1.84 | 1.91 | 1.99 | 2.09 | 2.22 | 1.98 | 2.06 | 2.15 | 2.30 |
| $r\omega$, in/sec | 597 | 572 | 544 | 515 | 485 | 449 | 542 | 513 | 483 | 447 |
| $\dot{L}$ | 557 | 506 | 446 | 397 | 344 | 290 | 420 | 377 | 327 | 273 |
| t,ms | 4.31 | 4.74 | 5.38 | 6.05 | 6.97 | 10.4 | 5.71 | 6.37 | 7.34 | 10.3 |
| Total ms | | | | | | 37.8 | | | | 29.7 |

TABLE 8 UNWINDING TIMES OF SHORTER RIBBONS

Ribbon thickness will affect unwinding time, according to the straight bridge model, by its effects on the geometry of r and $r_c$. To illustrate this, calculations are shown in Table 9 of 15 inch ribbons .002 inches thick and .006 inches thick (the .004 inch thickness is given in Table 8).

| h, in. | .002 | | | | | | .006 | | | | | |
|---|---|---|---|---|---|---|---|---|---|---|---|---|
| $\Delta L$ | 2.4 | 2.4 | 2.4 | 2.4 | 2.4 | 3.0 | 2.4 | 2.4 | 2.4 | 2.4 | 2.4 | 3.0 |
| Mean L,in | 13.8 | 11.4 | 9.0 | 6.6 | 4.2 | 1.5 | 13.8 | 11.4 | 9.0 | 6.6 | 4.2 | 1.5 |
| r, in. | .165 | .161 | .156 | .151 | .146 | .139 | .212 | .201 | .189 | .176 | .163 | .146 |
| $r_c$, in. | .341 | .339 | .336 | .334 | .332 | .329 | .339 | .332 | .325 | .319 | .312 | .304 |
| $r_c/r$ | 2.07 | 2.10 | 2.16 | 2.21 | 2.27 | 2.37 | 1.60 | 1.65 | 1.72 | 1.81 | 1.91 | 2.09 |
| $r\omega$, in/sec | 519 | 504 | 489 | 473 | 457 | 438 | 665 | 631 | 594 | 554 | 512 | 459 |
| $\dot{L}$ | 374 | 355 | 329 | 307 | 286 | 258 | 778 | 691 | 600 | 507 | 422 | 326 |
| t,ms | 6.42 | 6.75 | 7.30 | 7.81 | 8.40 | 11.6 | 3.08 | 3.47 | 4.00 | 4.73 | 5.68 | 9.21 |
| Total ms | | | | | | 48.3 | | | | | | 30.2 |

TABLE 9 UNWINDING TIME VS. THICKNESS

Ribbon unwinding time is predicted to be a strong function of ribbon thickness, according to the straight bridge model. This effect is produced because the ribbon thickness affects the r to $r_c$ space. However, ribbon thickness also affects ribbon stiffness, which is a factor not even considered in this model. The standing wave model discussed below, however, does contain stiffness effects.

## 4.2 The Standing Wave Model

A wave in a zero-stiffness string (or ribbon) moves with the following velocity:

$$V_s = (T/\rho A)^{\frac{1}{2}} \qquad \text{Eq. (25)}$$

where T is the tensile force, $\rho$ is density, and A is the cross-sectional area. For a straight bridge, as in Fig.9, the mass of the bridge is $\rho A(r_c^2-r^2)^{\frac{1}{2}}$. Entering $\rho A$ into Eq.25:

$$V_s = (T/m)^{\frac{1}{2}}(r_c^2-r^2)^{\frac{1}{4}} \qquad \text{Eq. (26)}$$

Combining Eq.26 with Eq.16 for T and Eqs.11 and 12 for $F_r$ and $F_c$:

$$(V_s/r\omega)^2 = \left(\frac{r_c^2-r^2}{r_c^2+3r^2}\right)^{\frac{1}{2}}\left[(r_c^2/r^2-1)^{\frac{1}{2}}(1+V_t/r\omega)^2+4V_r/r\omega\right] \qquad \text{Eq. (27)}$$

Taking $V_t/r\omega$ and $V_r/r\omega$ from Table 6, wave velocities $V_s/r\omega$ are calculated and presented in Table 10.

| $r_c/r$ | 1.2 | 1.5 | 2.0 | 2.5 | 2.9 |
|---|---|---|---|---|---|
| $V_t/r\omega$ | .212 | .146 | .0719 | .0270 | .00438 |
| $V_r/r\omega$ | .938 | .653 | .498 | .413 | .366 |
| $V_s/r\omega$ | 1.220 | 1.411 | 1.615 | 1.750 | 1.842 |

TABLE 10 VELOCITIES IN STANDING WAVE MODEL

These standing wave velocities are plotted in Fig.12 for comparison with $\dot{L}$ predicted by the straight bridge model. At most practical values of $r_c/r$, the standing wave model predicts higher unwinding velocities than does the straight bridge model. For comparisons of total unwinding times, the .004 inch thick ribbons with lengths of 22.5 inches, 15 inches, and 10 inches are calculated, as shown in Table 11, under the same conditions used in Tables 7 and 8.

| Ribbon Length, in. | 22.5 | 15.0 | 10.0 |
|---|---|---|---|
| Straight Bridge, ms | 45.3 | 37.8 | 29.7 |
| Standing Wave , ms | 26.2 | 18.0 | 12.3 |

TABLE 11 UNWINDING PREDICTION COMPARISON

Table 11 shows that unwinding times predicted by the standing wave model are approximately half those predicted by the straight bridge model.

Effects of ribbon stiffness on standing wave velocity may be estimated from Fig.13, which has been calculated from equations given by Morse (Ref.4). In Morse's notation Q is modulus of elasticity, k is the radius of gyration of the ribbon's section (equal to $h/(12)^{\frac{1}{2}}$), $\gamma$ is the forcing

FIG. 13 PHASE VELOCITY OF WAVES IN A RIBBON

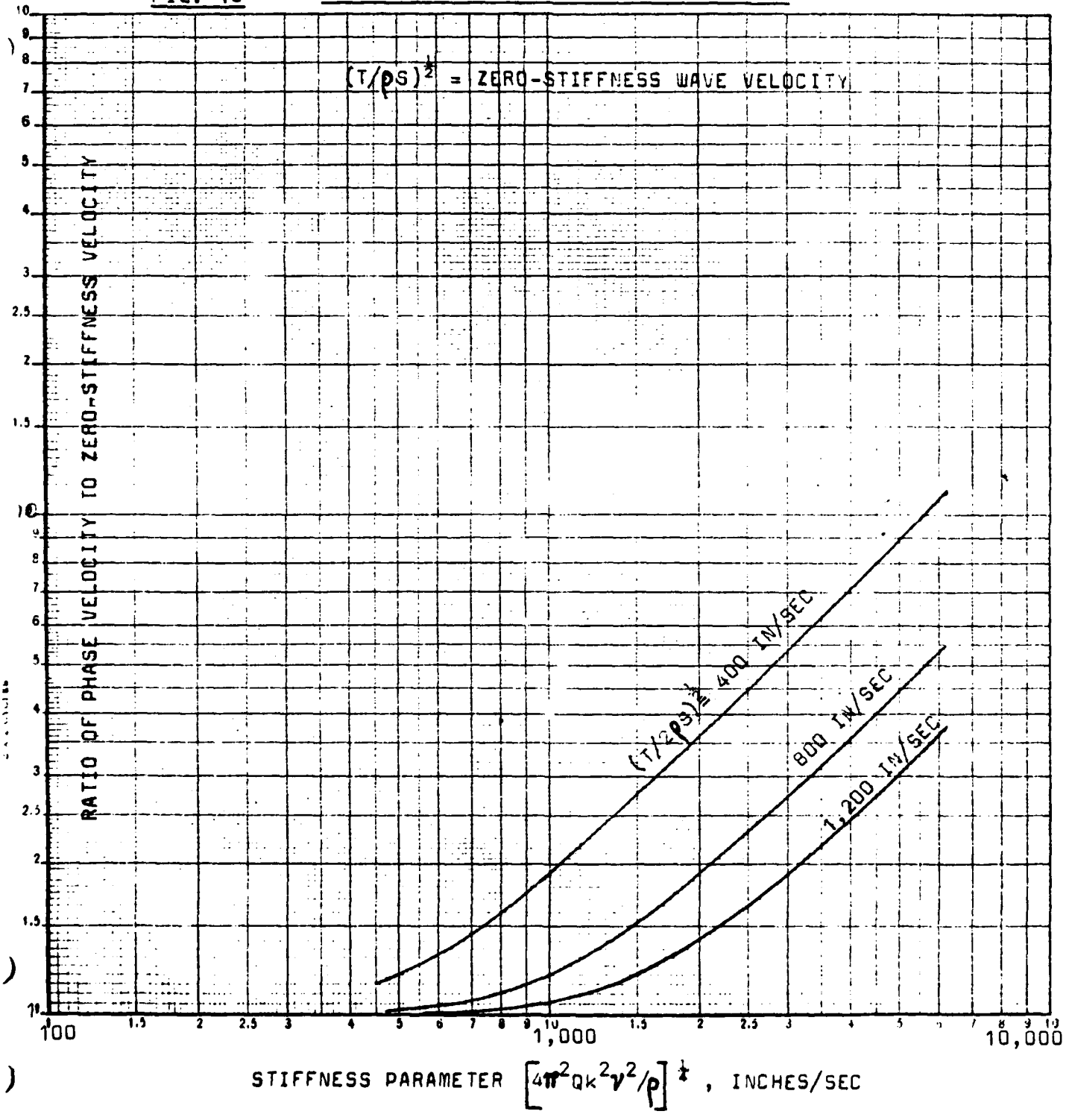

frequency (equal to $\omega$), and $\rho$ is density. For aluminum, the stiffness parameter used as the abscissa of Fig.13 is as follows ($\omega$ = 3142 rad/sec as in the previous examples):

$$\text{Stiffness} = \left[4\pi^2(10^7)\frac{h^2}{12}\frac{(3142)^2}{.10}/386\right]^{\frac{1}{2}} = 33{,}500\ h^{\frac{1}{2}},\ \text{in/sec}$$

In Table 12, stiffness parameters are applied to the 15 inch ribbons analyzed above in three different thicknesses. In each case the standing wave velocity is taken to be twice that calculated with the straight bridge model, for order of magnitude estimates.

| h, inches | .002 | .004 | .006 |
|---|---|---|---|
| Stiffness Parameter, in/sec | 1,500 | 2,100 | 2,600 |
| Est. $(T/\rho S)^{\frac{1}{2}} = L_o/t$, in/sec | 621 | 794 | 993 |
| $(T/2\rho S)^{\frac{1}{2}}$ | 439 | 561 | 702 |
| Approx. Velocity Ratio, from Fig.13 | 2.6 | 3.0 | 3.0 |

TABLE 12 EFFECTS OF STIFFNESS ON $V_s$

Table 12 indicates that stiffness can have a profound influence on unwinding speed, confirming the empirical observation that only dead-soft materials are suitable for ribbons. To isolate the effect of ribbon thickness on $V_s$ is a difficult task, however, since Fig.13 shows that such effects will depend on the magnitude of the stiffness parameter. At low values of the stiffness parameter, variations in h will have little effect.

Both theoretical models discussed above will be compared with empirical data. Absolute predictive capabilities will be calculated, as well as the abilities of the models to predict trends in unwinding times as affected by material, geometry, and other parameters. To aid in this evaluation process, total unwinding times have been calculated and plotted in Fig.14. Average values of r and $r_c$ during the unwinding process have been employed in calculating Fig.14, in order to avoid the step-by-step calculations such as those given in Tables 7-9. This averaging approach does not introduce excessive inaccuracy in $\Delta t$, and Fig.14 will be employed for comparing theoretical models with empirical results.

## 4.3 Correlations with Empirical Data

Fig.15 presents the empirical data obtained in this program (Section 2, Table 1) in the format suggested by the analytical models, i.e., $r_{co}\omega\Delta t/L_o$ vs. $hL_o/4\pi r_1 r_{co}$. To a first approximation, ribbon material does not seem to have much effect despite wide variations in density (from aluminum to lead) and other properties. Accordingly, a single curve is faired through the scattered data points. This curve is plotted in Fig.16 for comparison with the predictions of the two analytical models at the experimental $r_{co}/r_1 = 2.51$.

Fig.16 shows no distictly better predictive accuracy of one model over the other, with the empirical data falling between the two predictions at $r_{co}/r_1 = 2.51$.

In regard to the effects of $r_{co}/r_1$, which is predicted by the straight bridge model to have major effects and by the standing wave model to have relatively minor effects (see Fig.14), it is unfortunate that this distinct difference

FIG. 14 TOTAL UNWINDING TIMES

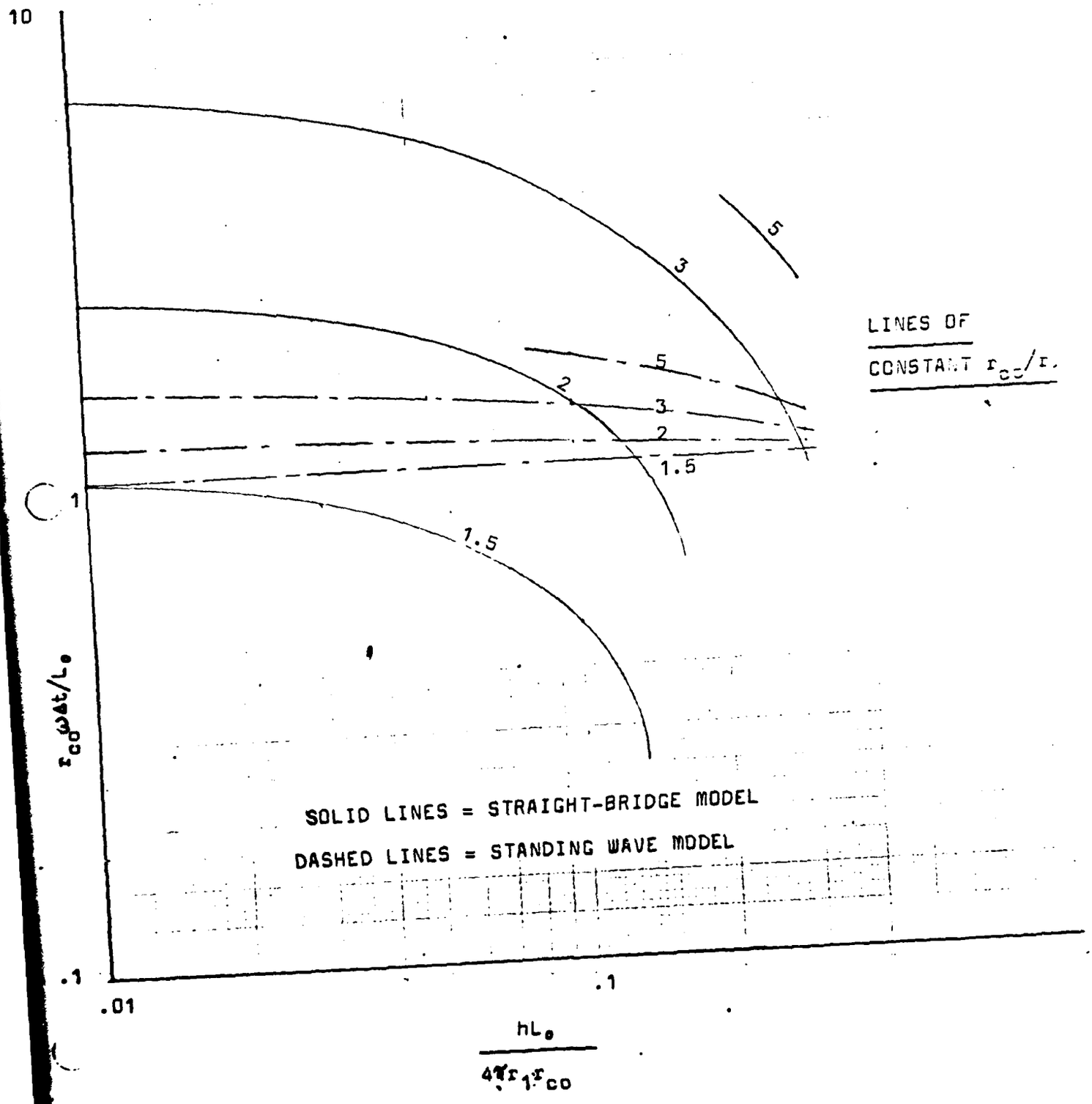


Logarithmic 2 x 2 cycles

FIG. 15 AIR SPINNER DATA WITH $r_{co}/r_1 = 2.51$

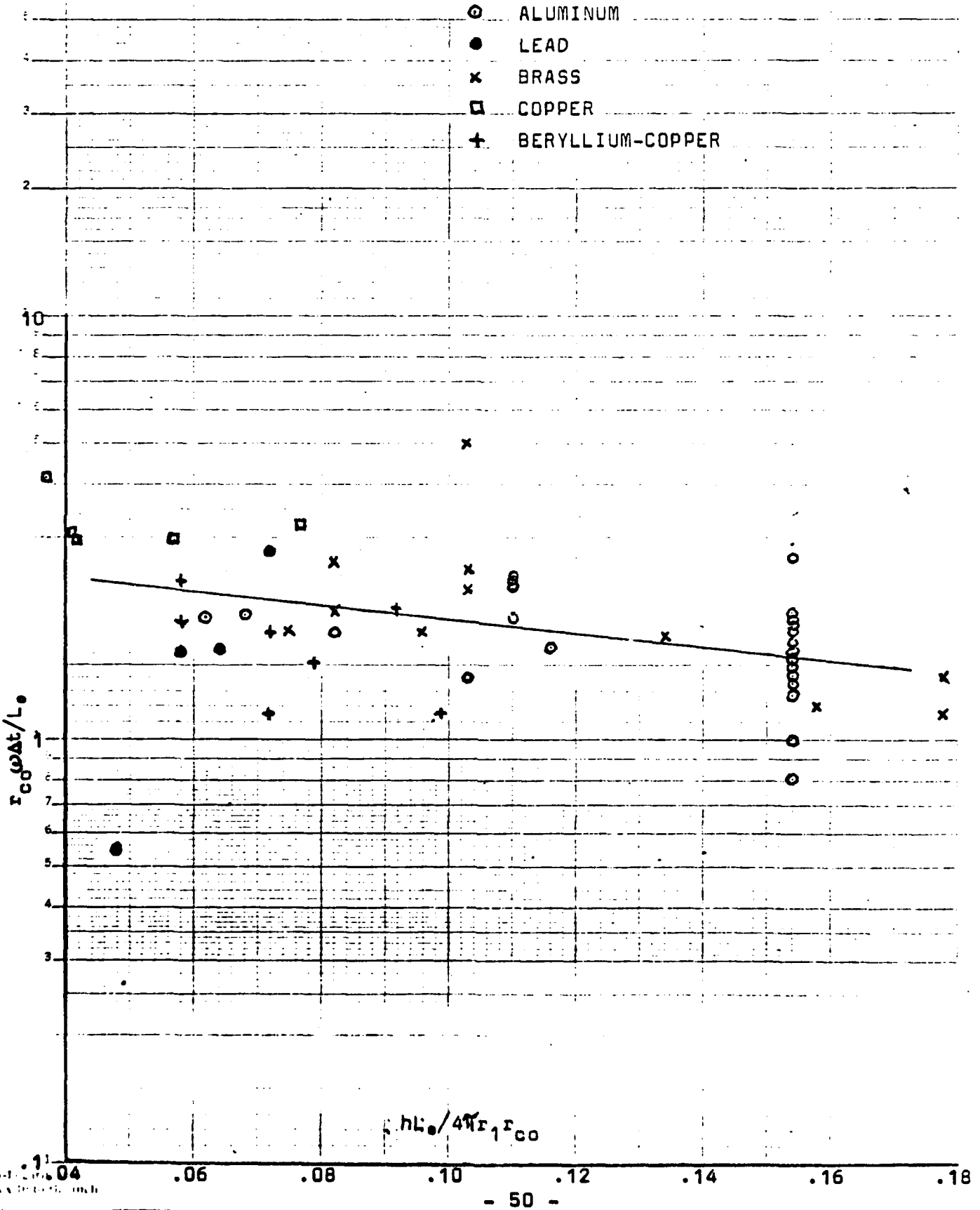

FIG. 16 COMPARISON OF MODELS AND DATA AT $r_{co}/r_1 = 2.51$

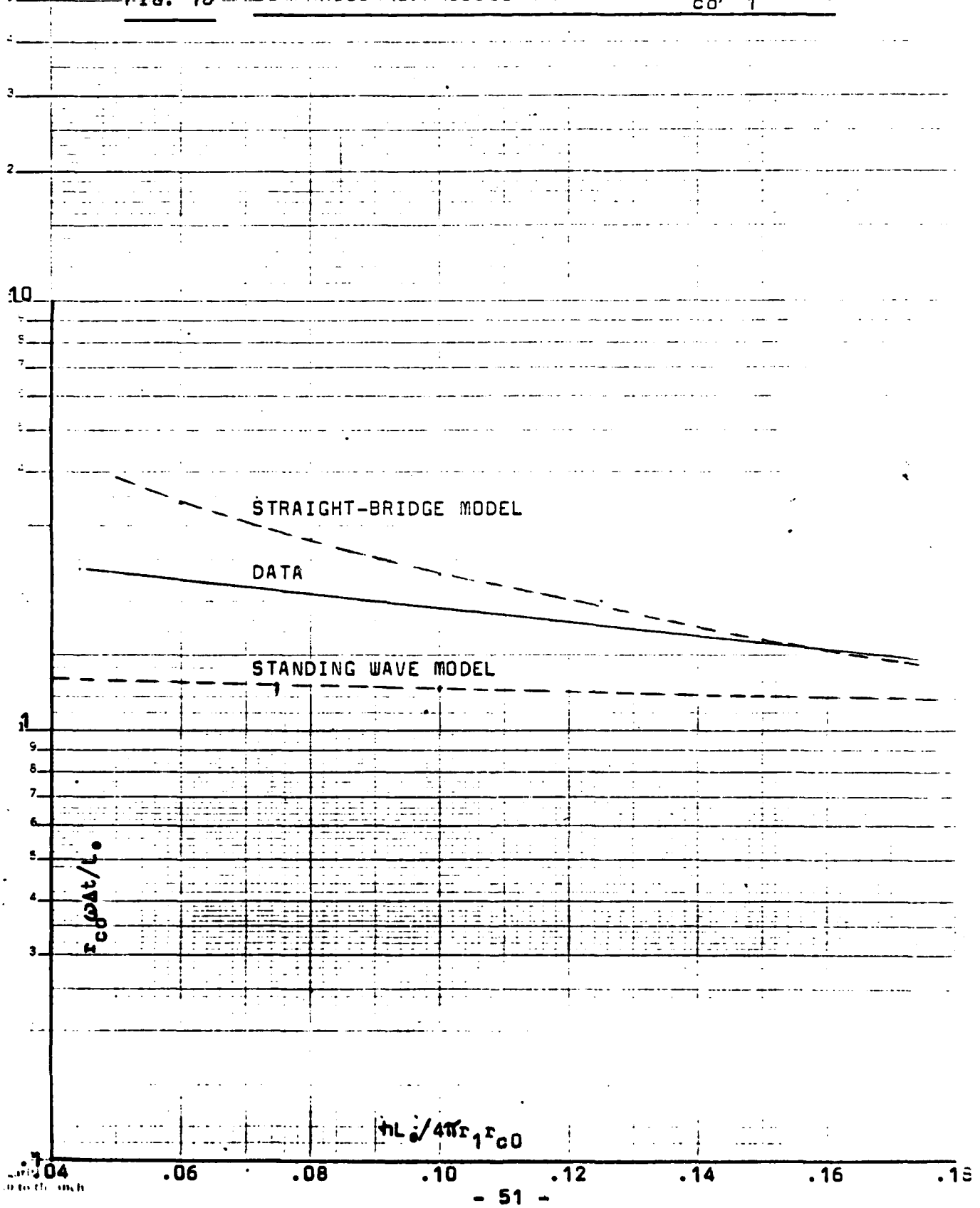

between the models cannot be evaluated on the basis of the $r_{co}/r_1 = 2.51$ air spinner data. The comparison of models can be made, however, on the basis of previously obtained data (Refs. 1,2) summarized in Table 2. These data are plotted in Fig.17 in groups of data, with each group having a constant $r_{co}/r_1$. Omitting for the moment the gun-fired unwinders and the with-liner ribbons (two thicknesses of .010 inch teflon liners between the hub and the innermost ribbon coil) which exhibit very high values of $r_{co}\omega\Delta t/L_o$, the remainder of the data tends to show negligible effects of $r_{co}/r_1$ in the 2.68 to 5.36 range. This lack of dependence on $r_{co}/r_1$ agrees with the standing wave model but conflicts with the predictions of the straight bridge model (see Fig.14).

Despite the reasonably good agreement between empirical data and the predictions of the standing wave model, this agreement does not establish the standing wave model as a physically complete description of ribbon dynamics. A basic dynamic analysis of ribbon motions during the unwinding process is required to establish the bridge shape, and how it may change as unwinding progresses.

## 4.4 Predictive Formula for Unwinding Time

Since Fig.17 shows that $r_{co}\omega\Delta t/L_o$ is practically independent of $r_{co}/r_1$, and the faired curve of Fig.16 shows a rather small effect of $hL_o/4\pi r_1 r_{co}$ (in the .04 to .18 range), it would appear that use of a mean value of $r_{co}\omega\Delta t/L_o$ may be adequate for purposes of designing ribbon unwinders. The air spinner data (Table 1) has a mean value of $r_{co}\omega\Delta t/L_o = 1.95$, which leads to the following equation for unwinding time:

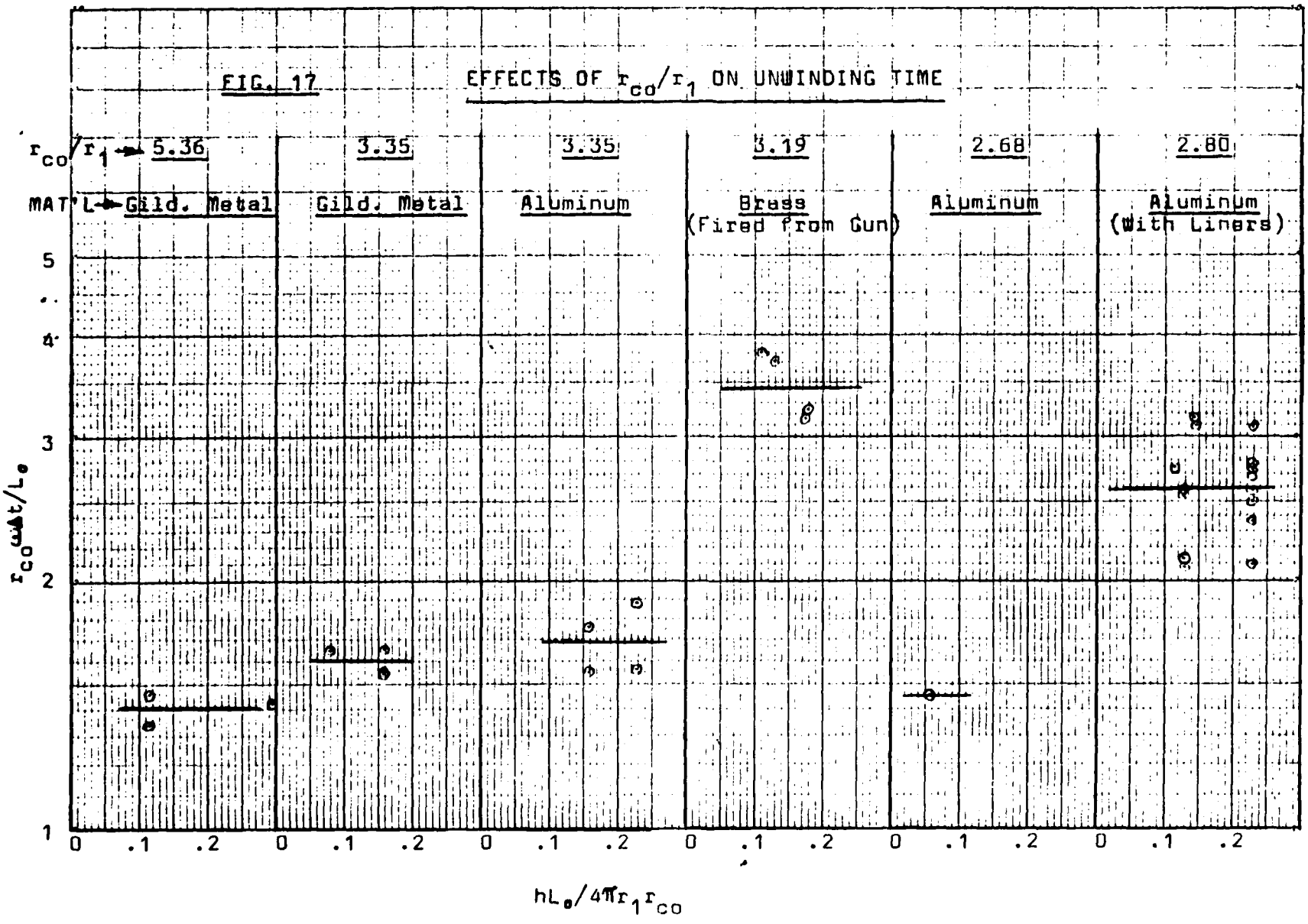
FIG. 17
EFFECTS OF $r_{co}/r_1$ ON UNWINDING TIME
$r_{co}/r_1$ → 5.36 3.35 3.35 3.19 2.68 2.80
MAT'L → Gild. Metal Gild. Metal Aluminum Brass (Fired from Gun) Aluminum Aluminum (With Liners)
$r_{co}\omega t/L_o$
1
2
3
4
5
0 .1 .2
$hL_o/4\pi r_1 r_{co}$

Unwinding Time $\Delta t = 1.95L_o/\omega r_{co}$ Eq. (28)

Applying Eq. 28 to all the empirical data gathered in this air spinner test program, it is found that the standard deviation is 0.76*. Since arming time requirements generally permit greater variability than standard deviation divided by mean = 0.76/1.95 = 0.39, Eq. 28 appears entirely adequate for designing ribbon unwinders for arming delay systems.

An interesting consequence of the form of Eq. 28 is that arming distance is a constant, regardless of muzzle velocity. For rifling with nd axial travel per revolution of the projectile (where d is projectile diameter) muzzle velocity = $\omega dn/2\pi$. Distance $S_a$ where arming occurs is muzzle velocity times $\Delta t$, or $\omega dn\Delta t/2\pi$. Since $\omega\Delta t = 1.95L_o/r_{co}$ from Eq. 28:

$$S_a/d = .31n(L_o/r_{co}) \qquad \text{Eq. (29)}$$

Further, as an order-of-magnitude generalization, $d/r_{co}$ will be approximately equal to 4:

$$S_a \cong nL_o \qquad \text{Eq. (30)}$$

For n between about 20 and 40, the arming distance of a ribbon unwinder will be of the order of 30 times the ribbon length.

---

* The ALN analysis (Chap. 3) showed that the data could not have resulted from random fluctuations. Therefore, calculating a "standard deviation" based on a normal distribution is not a rigorous procedure. However, applying this non-rigorous approach to Eq. 2 results in "standard deviation"/mean = 0.42.

## 5. CONCLUSIONS & RECOMMENDATIONS

The primary objective in this program of developing methods of designing ribbon unwinders has been to derive usable equations for predicting unwinding time. This objective is fulfilled to a good enough approximation by Eq. 28, which gives reasonable accuracy with only the parameters of ribbon length and outer cavity radius and spin rate, and to better accuracy by Eq. 2 which uses additional ribbon parameters. There is no doubt that these preliminary design equations can be improved by more comprehensive programs of experimentation and analysis, but it is believed that the methods developed here are accurate enough for evaluating the relative advantages of using a ribbon unwinder as a delay element in a particular application. Further refinement of these equations is recommended, however, in view of the small data base used in their development.

It must be emphasized that unwinding time is not the sole criterion for selecting ribbon material and thickness. Aluminum 1100-0 is considered an excellent material because of its dead soft condition without requirement for annealing. Lead is also quite soft; however, the consensus is that it is too soft to handle as a practical fuze component. Likewise, foil below about .002 inches (.05 mm) in thickness may prove difficult to handle and may also be susceptible to edge damage during setback.

Ribbons with a high thickness-density product may be required in some applications to overcome the adhesive stresses between the coil layers. Table 1 contains the examples of .0012 inch (.030 mm) aluminum that did not unwind at spin rates of the order of 30,000 rpm, .0015 inch (.038 mm) copper that did not unwind at 20,000 rpm, and

.004 inch (.102 mm) aluminum that did not unwind at 15,000 rpm. Calculations of the centrifugal stresses at the outermost layer of the ribbon coil ($r\omega^2\rho h$) were in the 0.5 to 1.0 psi range, and it is assumed that the adhesive stresses between the outermost ribbon turn and its adjacent turn were somewhat higher, thus preventing the ribbons from unwinding. Comparable data available from previous programs are 2.4 psi for a .006 inch (.152 mm) aluminum ribbon (Ref.1) and 7.4 psi for a .004 inch (.102 mm) brass ribbon (Ref.2). Inter-coil adhesive stresses are undoubtedly affected by the surface condition of the ribbon, and it may well be that the relatively low stresses obtained in this program were due to the use of magnesium oxide on one side of each ribbon to assist in annealing. In any event, it may be a practical necessity to measure inter-coil adhesive stress for each candidate ribbon material and then make sure that $r\omega^2\rho h$ exceeds the measured stress.

Ribbon unwinders appear to offer such good advantages as delay elements that a considerable amount of effort to develop unwinder technology is recommended. Some promising areas of study that can be expected to broaden the data base and to yield further insights into the behavior of ribbon unwinders are as follows:

(1) Development of a computer model of ribbon unwinder dynamics, including bending stiffness and adhesive stresses and friction, from the time of release of the ribbon's free end until the entire ribbon is transferred to the outer cavity wall.

(2) Spinner experimentation with variations in the parameters that were held constant in this program, particularly hub and cavity radius.

(3) Setback experimentation that may reveal the time delay required to spin up the coil, any effects of setback on the edges of the ribbon, and any effects the shock and vibration environment inside the spinning projectile may have on the ribbon unwinding process.

Perhaps the single most important reason for continuing careful analytical and experimental programs such as the above is that much-needed experience will be gained with an arming delay system that shows such promise.

## APPENDIX A

### ADAPTIVE LEARNING NETWORK METHOD

Adaptive Learning Networks (ALNs) is an area of Artificial Intelligence that is concerned with producing phenomenological models of physical processes. The method for producing ALN models has been highly developed by ADI and has been successfully applied to such modeling problems as detection, classification, parameter estimation, prediction, process control, and others. For the ribbon unwinding data, the ALN can be used to model the unwinding time.

The classical approach to problems of detection, classification, estimation, etc. has been to determine explicitly all of the relevant characteristics (deterministic and/or statistical) of the observed process and to use those measurements and assumptions in the synthesis of a model. Often, the mathematical structure of the true process is assumed and the design process consists of calculating the coefficients of the model equations.

In many cases, the inputs or observables cannot be related to the output of the process in an analytical fashion. Further, the best or even an acceptable structure for the model cannot be determined a priori. These facts often result in linear models being used simply because the mathematics of such models are tractable.

However, it is often desirable to implement the model of a particular process as a general (usually nonlinear) function of certain input variables, the observables or features. Since the details of the relationships between the input variables and the output variable (the output process) are not known, the parameters and structure of the model are not known a priori. Rather, the model has to be "trained" from a data base of representative inputs and corresponding outputs.

To achieve trainability, the Adaptive Learning Network procedure uses, as a model of the observed process, a network of similar elementary building blocks. The training, or model synthesis, process determines the number of the elementary building blocks, the interconnections between them, and the parameters in each. In this way, the structure and coefficients of the model are derived from observations of the process. In order to implement such a scheme, the following questions need to be considered: First, what should the structure of the elements of the network be? Second, how should the element parameters be adjusted; and third, how should the elements be interconnected and what should be their complexity (i.e., number)?

These questions can be more clearly understood as follows: suppose that the process input consists of N observables, $x_1, x_2, \ldots, x_N$. Also, suppose that the output y is a scalar whose value may be considered as the estimate of some property of the input process. For the present application, that value is the ribbon unwinding time. In general, y will be some nonlinear function of the $x_i$'s, as follows:

$$Y = f(x_1, x_2, \ldots, x_N) \qquad (A.1)$$

Under fairly general conditions, a function of N variables may be expressed in an N-dimensional series as follows:

$$y = a_0 + \sum_{i=1}^{N} a_i x_i + \sum_{i=1}^{N}\sum_{j=1}^{N} a_{ij} x_i x_j + \sum_{i=1}^{N}\sum_{j=1}^{N}\sum_{k=1}^{N} a_{ijk} x_i x_j x_k + \ldots \qquad (A.2)$$

In the most general case, the coefficients, $a_0, a_1, \ldots$, are functions of time, but for many cases of interest, the underlying characteristics of the x's do not depend on time and, consequently, the coefficients are constants.

The above-stated questions can now be restated in terms of Equation (A.2) as follows: What elemental polynomial of the $x_i$'s can be chosen such that, when its coefficients are adjusted and when several of them are interconnected, the resulting network is a good approximation to Equation (A.2) for the process of interest? Experience has shown that the element polynomials can be chosen to be either two-input or three-input devices. The three-input element implements a nonlinear function of inputs $x_1$, $x_2$, and $x_3$:

$$y = w_0 + w_1x_1 + w_2x_2 + w_3x_3 + w_4x_1x_2 + w_5x_1x_3 + w_6x_2x_3 + w_7x_1^2 + w_8x_2^2 + w_9x_3^2 + w_{10}x_1x_2x_3 + w_{11}x_1^3 + w_{12}x_2^3 + w_{13}x_3^3 \quad \text{(A.3)}$$

To reduce computational complexity, only one element of each layer of the network is allowed to use three inputs. Most elements contain only two inputs ($x_1$, $x_2$) such that:

$$y = w_0 + w_1x_1 + w_2x_2 + w_4x_1x_2 + w_7x_1^2 + w_8x_2^2 + w_{11}x_1^3 + w_{12}x_2^3 \quad \text{(A.4)}$$

A network of two layers of basic elements can contain products up to the ninth degree. Thus, fairly complex multinomials can be built up in a few network layers. To implement a fully general multinomial as in Equation (A.2), the number of elements in each layer would have to grow as one adds additional layers to the network. However, it has been found empirically that for most physical processes, acceptable networks can be obtained without such growth; in fact, the number of elements in successive layers decreases, and only a few layers are needed in the final network.

The coefficients in Equations (A.3) and (A.4), the $w_i$'s are determined for each element individually by least squares fitting the desired or observed output y to the chosen inputs, $x_i$. The process of determining these coefficients and the number and interconnection of the individual elements is called the training of the ALN. These tasks are accomplished with a data base, for which the values of the dependent and independent variables are known. The steps involved in this process are:

(1) optimization of the coefficients in each element of the first layer;
(2) selection of those elements whose output is acceptable while rejecting poor performers;

(3) repetition of the first two steps for consecutive layers of the network;

(4) determination of the optimum number of network layers; and

(5) global optimization of all coefficients in all layers.

There are two ways in which step 4, the determination of the optimum number of network layers, can be performed. The first is an empirical technique which requires that the known data base be divided into three independent but statistically similar subsets called the fitting, selection, and evaluation subsets. The second technique makes use of an information theoretic criteria and requires only two subsets, a fitting subset and an evaluation subset. The division of the data base into subsets is accomplished with the Mucciardi-Gose clustering algorithm (Mucciardi and Gose, 1972). In both cases, the fitting subset is used to determine the coefficients of the elements. For the information theoretic criteria approach, the fitting subset is also used to reject those features that perform poorly. For the empirical approach, the selection subset is used to reject the poor performers and to prevent overfitting. Also, for that case, the fitting and selection subsets are used for the global optimization. The purpose of the evaluation subset is to estimate the overall performance. Since the evaluation subset is not used for network synthesis, the performance of this subset is an accurate estimate of the ability of the network to generalize to new, previously unseen data.

Consider, for the following, that each element has only two inputs and that the empirical technique for the determination of the correct number of layers in the network is being used. Then the fitting and selection subsets are used alternately in training each layer. First, the N-specific observables are arranged into N(N-1)/2 pairs, feeding a like number of trainable elements. Then the fitting subset of the known data base is applied to establish the coefficients, using a recursive search procedure to minimize the error rate between the independent variables and the output of the basic elements. The procedure is repeated for each of the N(N-2)/2 elements. Not all pairwise combinations are significant in extracting the desired information. The selection process, using the selection subset, eliminates those elements whose performance is not acceptable, as gauged by the error criterion. There are now, say, R elements that survive. The process is repeated for the second

layer. The observables now consist of the outputs of the surviving elements as well as the original independent variables. Coefficients of each element in the second layer are determined as in the first layer. Then the selection subset is fed a second time into the first layer and the unacceptable pairs eliminated from the second layer.

This process can be repeated with succeeding layers. In addition to eliminating the poorly performing features, the selection set is also used for determination of the optimum number of layers. The selection set should be used for this purpose because the error rate on the fitting subset could be continuously decreased by incorporating additional layers. Overfitting of the fitting subset occurs when the error rate on the selection subset starts increasing. Avoidance of overfitting is a key aspect in the training of learning networks (Ivakhnenko, 1971; Mucciardi, 1972). The network must be thought to generalize properly on its experience in fitting the points in the fitting subset, so that error rates in later uses for statistically similar data will also be low. The network may produce deceptively small errors in approximating the fitting subset and then do poorly on subsequent new data when overfitting is not avoided.

The growth of the model, i.e., the increase in the number of coefficients, can also be controlled by the use of an information criierion such as AIC, also called Akaike's information criterion (Akaike, 1973 and 1980; Kondo and Tamura, 1980; Tamura and Kondo, 1980). AIC measures the poorness of the model and, consequently, needs to be minimized:

$$\text{AIC} = 2\ell n(\text{maximum likelihood}) + 2(\text{number of coefficients}) = \text{minimum}. \quad \text{(A.5)}$$

In this case, the resulting model is called the minimum AIC model (MAIC). AIC is an estimate of twice the negentropy: thus a realization of the MAIC model is equivalent to the finding of that model from all possible models which possess the maximum entropy. AIC has also been used in autoregressive analysis techniques, such as spectral estimation; the optimal length for the prediction filter can be determined by applying AIC (Ulrych and Bishop, 1975; Landers and Lacoss, 1977).

When the appropriate number of layers has been found, the last layer will, in general, comprise a plurality of elements, each capable of producing an estimate of the dependent variable. These estimates may be numerically weighted and summed, or the single element that produces the lowest error rate vis-a-vis the selection subset may be retained, while all other parts of the network not needed to feed the surviving output element or elements are discarded.

A final step in the training process is the global optimization, also called vernier adjustment, of the coefficients. This may be desirable because the coefficients of each element have been adjusted in the absence of interactions with other elements following them in the network; optimum coefficient values may be slightly different from those determined earlier when these interactions are present. Fitting and selection subsets are also used for this final adjustment process. The vernier adjustment uses a random technique to obtain the optimum values of the coefficients, as well as for subsequent network adaptation. After final adjustment of the coefficients, the evaluation subset is used to estimate performance of the entire network.

In summary, the ALN technique is an empirically-based technique to obtain the structure of a process and does not require a priori principles and/or assumptions to be made about the process itself. Since both the structure of the model and the values for the model coefficients are obtained from the experimental data base, the ALN method is applicable to multi-sensor integration, detection classification, prediction, and the control of a wide range of complex physical, biological, and engineering processes. Application of ALN modeling has been successful even when theoretical or conventional modeling techniques produced insufficient results.

## REFERENCES


1. Raff, B. and R.J. Caruso "Design and Development of Fuze, PIBD, XM579" Bulova Final Report, 19 Dec. 1969.

2. Tevelow, F.L. "Terminal Report - T362 Octopus Fuze" Diamond Ordnance Fuze Laboratory Report TR-673, 10 August 1959.

3. Alfriend, T.B. "Study of Wrapped Springs for Application to a Delayed Arming Mechanism" Aircraft Armaments Inc. Report No. ER-1404, June 1958.

4. Morse, P.M. "Vibration and Sound", McGraw-Hill, Second Ed., 1948.

5. Hogg, R.V. and A.T. Craig "Introduction to Mathematical Statistics", Second Ed.,p. 291, McMillan, New York, 1965.